TEKNILLINEN TIEDEKUNTA

GEOPOLYMERS AS MEMBRANE FILTRATION MATERIALS

Elisa Olsen

Process Engineering

Master's thesis

July 2021

TIIVISTELMÄ

Geopolymers As Membrane Filtration Materials

Elisa Olsen

Oulun yliopisto, Prosessitekniikan tutkinto-ohjelma

Diplomityö 2021, 73 s.

Työn ohjaajat yliopistolla: Tero Luukkonen & Esa Muurinen

Tämän diplomityön tavoitteena oli tutkia geopolymeerien soveltuvuutta kalvosuodatusmateriaaliksi. Työssä tutkittiin alkaliaktivoidusta metakaoliinista sekä masuunikuonasta valmistettujen geopolymeerikalvojen ominaisuuksia erilaisin karakterisointimenetelmin ja suoritettiin suodatuskokeita kalvojen erotuskyvyn määrittämiseksi.

Työn ensimmäisessä vaiheessa valmistettiin geopolymeerikalvoja, ja tutkittiin kalvomateriaalin ominaisuuksia, kuten mineralogiaa, rakennetta, huokoisuutta, zeta-potentiaalia sekä mekaanista kestävyyttä. Työssä tutkittiin myös eri lämpötiloissa suoritettujen lämpökäsittelyiden sekä hydrotermisen käsittelyn vaikutusta kalvomateriaalin rakenteeseen. Työn toisessa vaiheessa valmistettuja kalvoja käytettiin ultrasuodatuskalvoina, ja niillä pyrittiin erottamaan vesiliuoksesta humushappoa ja ammoniumioneja. Suodatuskokeissa selvitettiin myös lämpötilan ja paineen vaikutusta kalvon läpäisevään vesivuohon.

Suodatuskokeissa havaittiin, että geopolymeerikalvoja voidaan käyttää ultrasuodatuksen kalvomateriaaleina. Sekä metakaoliini- että masuunikuona- ja metakaoliinipohjaisilla geopolymeerikalvoilla onnistuttiin erottamaan ammoniumioneja vesiliuoksesta. Humushapposuodatuksissa havaittiin, että kalvon läpäisevät permeaattinäytteet kontaminoituvat kalvosta tai suodatuslaitteistosta, eikä selkeitä johtopäätöksiä kalvojen soveltuvuudesta orgaanisen aineksen erottamiseen voida tehdä.

Asiasanat: alkaliaktivoidut materiaalit, geopolymeerit, kalvosuodatus

ABSTRACT

Geopolymers As Membrane Filtration Materials

Elisa Olsen

University of Oulu, Degree Programme of Process Engineering

Master's thesis + 2021, 73 pp.

Supervisors at the university: Tero Luukkonen, Esa Muurinen

The aim of this thesis was to study the suitability of geopolymers as membrane filtration materials. In the thesis, the properties alkali-activated metakaolin- and blast furnace slag -based geopolymer membranes were investigated with a variety of characterization methods, and a set of filtration experiments was conducted to determine the separation performance of the membranes.

In the first stage of the thesis, geopolymer membranes were prepared and the properties, such as mineralogy, structure, porosity, zeta potential, and mechanical durability, of the membrane materials were studied. The effects of sintering at different temperatures and hydrothermal treatment on the material were also investigated. In the second stage of the work, the prepared membranes were used for membrane filtration, and the goal was to separate humic acid and ammonium ions from aqueous solutions. The effect of temperature and pressure on the water flux through the membranes was also investigated in the filtration experiments.

The main finding of the filtration experiments was that geopolymer membranes can be used in ultrafiltration. Both metakaolin, and metakaolin- and blast furnace slag -based membranes were able to separate ammonium ions from aqueous solutions. In humic acid filtrations, it was observed that the permeate samples were contaminated from the membrane or the filtration unit, and clear conclusions from the applicability of the membranes to separation of organic matter cannot be drawn.

Keywords: alkali-activated materials, geopolymers, membrane filtration

FOREWORD

The purpose of this thesis was to study geopolymers as membrane filtration materials. The work was carried out for Fibre and particle engineering unit at the University of Oulu between January and July, 2021.

First, I want to thank my supervisors, assistant professor Tero Luukkonen and docent Esa Muurinen, for giving me the opportunity to write this thesis, and for instructing and guiding me through the process.

I want to express my gratitude for the whole staff of the Fibre and particle engineering unit laboratory for their help and advice during the experimental phase. I'm especially grateful for laboratory technicians Elisa Wirkkala, Jani Österlund and Jarno Karvonen, for their invaluable guidance and assistance with all the laboratory equipment. I'm very thankful for planner Auli Turkki from Environmental and chemical engineering unit, for providing precious tehcnical support. I highly appreciate all the help I have gotten from different research units with the equipment, experiments and analyses.

Words cannot describe how grateful I am for my family and friends for their support, encouragement, and love.

Keminmaa, 29.7.2021

Elisa Olsen
Elisa Olsen

TABLE OF CONTENTS

1 INTRODUCTION

Pressure-driven membrane processes like reverse osmosis and ultrafiltration are widely utilized for drinking water purification and desalination. The low cost and energy efficiency of membrane processes enhance their competitiveness against conventional industrial separation and water purification processes, such as distillation and chemical purification methods (Moulik et al. 2019, 7-10). As water is an essential and precious resource and the world's population and demand for fresh water is ever-growing, the race for developing efficient, low-cost water purification processes is fiercer than ever before.

The main pollutants in industrial and municipal wastewaters in Finland are suspended solids, adsorbable organic halides (AOX), phosphorus, nitrogen, and organic matter, which is typically expressed by biological oxygen demand (BOD) and chemical oxygen demand (COD). Pulp and paper industry, metal industry and chemical industry are the most significant industrial sources of wastewater pollutants by producing over 90 % of the total industrial nitrogen, BOD and COD emissions in the water (Finland's Environmental Administration 2021).

The focus pollutants of this work are nitrogen and humic acid. Nitrogen is present in wastewaters in the forms of nitrite (NO_2^-), nitrate (NO_3^-), ammonia (NH_3) and ammonium (NH_4^+). The main source of nitrogen in wastewaters is urea from urine and proteins from faeces (Metcalf & Eddy et al. 2014). Humic substances are organic matter that are present in natural waters and soil naturally. Humic substances are not essentially pollutants, but the presence of humic substances, such as humic acid, in water causes unpleasant brownish colour and mud-like odour and taste. Humic substances also indirectly impair the sanitary quality of water by consuming water disinfectant chemicals and binding pollutants (e.g., heavy metals and pesticides) in the water. The oxidation reactions of humic acid yield hazardous, carcinogenic halogenated compounds, and the removal of humic substances from water increases the efficiency of the overall water purification process and the quality and safety of potable water. (Lin et al. 2012; Zhao et al. 2019; Yang et al. 2019)

The key disadvantage hindering yet wider use of membrane technology for water purification are the physical and chemical properties of the membranes: Polymeric

membranes are an economically feasible option, but poor mechanical, chemical, and thermal durability of the materials sets limitations for the operating conditions (Madaerni et al. 2015, s. 3). Ceramic membranes can endure harsh conditions and have long life cycles, but the production costs are high, mainly due to the energy consumption of the high temperature production process (Lee et al. 2015, s. 44). Novel ceramic-like materials, such as alkali-activated materials, are a promising alternative, as the production costs are lower than in ceramic membranes, the raw materials are low-cost industrial wastes or by-products, and the chemical, mechanical and thermal stability can be higher than with polymeric membranes.

Alkali-activated materials are prepared by introducing an alkali activator, typically a solution of sodium or potassium hydroxide and silicate, to an aluminosilicate precursor. Metakaolin, fly ash and blast furnace slag are commonly used aluminosilicate precursors. The product of the synthesis is a micro- ($d_0 < 2$ nm) or mesoporous (2 nm $\leq d_0 \leq$ 50 nm), mechanically strong, and chemically inert 3D-network structure on nanometer scale. (Ge et al. 2015; Xu et al. 2019; Della Rocca et al. 2020). Alkali-activated materials have been successfully synthesized and used in membrane processes, e.g., desalination by pervaporation (He et al. 2013), removal of suspended solids from green liquor (Xu et al. 2019) and separation of water and ethanol by pervaporation (Azarshab et al. 2016).

The theoretical framework of the study revolves around membrane filtration and alkali-activated materials. The raw materials, structure, physical and chemical properties, and terminology of alkali-activated materials are discussed in chapter 2, and chapter 3 presents the principles and applications of membrane separation processes. Previous studies of the application of alkali-activated materials in membrane filtration are also introduced in chapter 3.

The experimental part of the work focuses on the preparation of geopolymer membranes and characterization of the produced membranes. The properties and suitability of alkali-activated materials for membrane filtration were investigated by a series of analyses, such as zeta-potential analysis, scanning electron microscopy (SEM), X-ray diffraction (XRD), and analysis of specific surface area and nanoscale porosity by Brunauer-Emmet-Teller (BET) isotherm and Barrett-Joyner-Halenda (BJH) method. The membrane materials were subjected to thermal treatments: One-hour sintering at 700°C to convert the

geopolymers to high temperature ceramics; one-hour sintering at 300°C to finalize the geopolymerization reactions; or 15-hour hydrothermal aging in a water bath in 90°C to convert the geopolymers to zeolites. The effects of sintering (700°C, 300°C) and hydrothermal aging (water bath in 90°C) were investigated with XRD, BET and BJH. The analysis methods will be further explained in chapter 4.

The water flux of the prepared membranes was studied by filtrating pure, de-ionized water in different temperatures and pressures. Filtrations with 0.1 M acetic acid were done to neutralize the pore solution of characteristically alkaline membranes. Filtration experiments with humic acid and ammonium ion solutions were performed to study if alkali-activated materials can separate humic acid molecules as measured by reduction in total organic carbon (TOC) and ammonium ion concentration of wastewaters. The results of analyses and filtration experiments are presented in chapter 5.

2 ALKALI-ACTIVATED MATERIALS

Alkali and industrial slags as components of cementing materials have intrigued inventors and researchers since the 19th century – in 1895, United States Patent No. 544706 was issued to Jasper Whiting of Chicago, Illinois, covering the use of caustic soda, potash, sodium chloride or equivalents, as an aqueous solution or dry state, at any stage of slag-cement manufacture. After decades of research, it was discovered that binders and cements can be produced from aluminosilicate clays using alkali metal solutions. Finally, in 1970's the inventor of the term "geopolymers", French materials scientist Joseph Davidovits, further developed the concept of producing binders by mixing alkalis with kaolinite, dolomite, and limestone (Shi et al. 2006). According to Davidovits, the inspiration for researching inorganic, heat-resistant, plastic-like materials originated from a series of catastrophic fires in France in the beginning of 1970's (Davidovits 1991).

"Geopolymer" is the established term for solid aluminosilicate materials that have been synthetized by activating a low-calcium precursor, e.g., metakaolin or fly ash, by alkali hydroxide or alkali silicate. Alkali-activated materials is a more generic term that covers also materials prepared of high-calcium precursors, such as blast furnace slag. A variety of other terms and names have been used: For example, names like "inorganic polymers", "soil cements" and "mineral polymers" have been introduced. (Provis 2014)

Even though the research on alkali-activated materials has focused on finding eco-friendly and low-cost alternatives for cementitious binders in construction purposes (Provis et al. 2014), a variety of other potential uses for alkali-activated materials have caught the interest of researchers. Due to the porosity, stability, mechanical strength, and electrostatic properties of alkali-activated materials, they have multiple potential applications in wastewater management, including adsorption of metal and heavy metal ions, photocatalysis, membrane filtration, antimicrobial filters and solidification and stabilization of water or wastewater treatment residues, such as sludges or ion-exchange resins (Jia et al. 2020; Luukkonen et al. 2019).

2.1 Alkali-activation

Alkali-activated materials are produced by mixing an alkaline activator solution, typically potassium or sodium hydroxide or silicate, with an aluminosilicate. The mixture forms a gel that sets and hardens in mild conditions. Alkali-activated materials are typically divided to two groups, high-calcium, and low-calcium materials, depending on the nature of the aluminosilicate (Garcia-Lodeiro et al. 2015). However, also intermediate forms combining low and high-calcium materials exist.

2.1.1 High-calcium materials

Blast furnace slag (BFS) is formed as a by-product of iron production, as the iron ore is reduced to iron and the remaining components from the ore form a slag, that is extracted from the furnace. The main components of blast furnace slag are calcium, aluminium, magnesium, and silica compounds, depending on the origin of the ore. Blast furnace slag is the most commonly used and abundant, high-calcium material used in alkali-activation (Shi et al. 2006). The average composition of blast furnace slag in Finland is presented in Table 1.

Table 1. Average composition of blast furnace slag in Finland (Finnsementti 2019).

	CaO	SiO_2	Al_2O_3	MgO	S	Ti	K_2O	Na_2O
Mass- %	36.0 – 42.0	36.0 – 42.0	8.0 – 10.0	10.0 – 12.0	1.5 – 2.0	0.9 – 1.3	0.5 – 1.0	0.5 – 1.0

Several factors affect the hydraulic reactivity and activity of blast furnace slag in alkali-activation: glass content, fineness, and chemical and mineralogical composition. Blast furnace slag consists of both vitreous and crystalline phases. The vitreous content of blast furnace slag has an influence on the hydraulic reactivity of the slag – however, research is not quite unanimous on the correlation between glass content and reactivity. Generally, the vitreous phase content should be over 90 %. Fineness of the slag has a clearer correlation to the reactivity of the slag; Small particle size increases the specific surface area, which results in better strength properties and reactivity. Another important factor is the pH of the slag: Hydraulic activity is higher for basic slags. The mass ratio of CaO and MgO to SiO_2 should be greater than 1 to ensure high basicity. (Pal et al. 2003)

The reaction mechanism for alkali-activation of calcium- and silica-rich materials has been proposed by Glukhovsky and Krivenko (1967, 1994; cited by Garcia-Lodeiro et al. 2015). In the proposed reaction mechanism shown below in Eq. 1, the alkaline cation (R^+) catalyses the initial phases of hydration via cationic exchange with the Ca^{2+} ions.

$$\begin{aligned} &SiO^- + R^+ \rightarrow SiOR \\ &SiOR + OH^- \rightarrow SiOROH^- \\ &SiOROH^- + Ca^{2+} \rightarrow SiOCaOH + R^+ \end{aligned} \quad (1)$$

The reaction produces an aluminium-containing calcium silicate hydrate gel, commonly referenced in the cement chemist notation as C-A-S-H gel. The exact composition and structure of the C-A-S-H gel depend on the curing conditions, the used alkali activator and the structure, origin, and composition of the blast furnace slag. For example, hydrotalcite phases can be present in the obtained alkali-activated material. (Garcia-Lodeiro et al. 2015)

2.1.2 Low-calcium materials

Metakaolin and class F fly ashes are common low-calcium materials that can be used in alkali-activation. Calcined clays, including metakaolin, were the first materials to be referred to with the term “geopolymer” (Davidovits, 2015). Metakaolin is derived from natural minerals: Weathering of feldspar produces kaolinite clay (Hillel et al. 2004), and calcination of kaolinite clay in 600 – 800°C breaks the structure of kaolin to metakaolin, which is a pozzolanic, highly reactive amorphous material (Rashad 2013) that consists of buckled silicate and aluminate layers (Provis et al. 2009). The downfall of metakaolin as material for alkali-activation is the high production costs caused by the high-temperature calcination of kaolinite – many other suitable materials are industrial wastes or by-products that have undergone high temperature during their formation (Garcia-Lodeiro et al. 2015).

Metakaolin typically contains 50 – 55 % silica species and 40 – 45 % alumina species. Some other oxides – such as CaO, MgO, TiO_2 and Fe_2O_3 - may be present in small quantities (Rashad 2013). The reaction mechanism of metakaolin based geopolymers can generally be divided into four distinctive stages. In the first stage, metakaolin is dissolved by the alkali activator, which leads to the release of silicate and aluminate species. In the

second stage, the released species react with the silicates from the activator solution to form aluminosilicate oligomers, which form an aluminosilicate gel in the third stage. The curing process is considered as the fourth and final stage of the reaction. Main reaction product is alkaline aluminosilicate hydrate, N-A-S-H, gel. (Kim et al. 2020; Van Deventer et al. 2007)

The final composition, properties, and microstructure of the obtained geopolymer product depend on type of alkali-activator, raw materials and curing conditions. For example, the porosity of geopolymers can be influenced by the molar ratios of the raw materials, and the density and degree of polymerization are dependent on the curing time and temperature (Benavent et al. 2016; Ivanovic et al. 2020). Generally, the curing temperature for metakaolin geopolymers is in the range of 60 – 200°C (Garcia-Lodeiro et al. 2015). However, ambient and near ambient curing temperatures can also produce geopolymers with satisfactory strength and microstructure (Bernal et al. 2014).

3 MEMBRANE SEPARATION PROCESSES

In membrane separation processes, a feed stream is divided into two fractions: Permeate, which passes through the membrane, and retentate, which is retained by the membrane. The mechanism of mass transfer through the membrane depends on the type and structure of the membrane: Highly porous membranes resemble conventional filters and retain particles based on the pore size distribution of the membrane. For non-porous, dense membranes, the mass transfer and separation performance of the membrane are related to the interactions, mainly diffusivity and solubility, between the membrane and the components of the feed. The permeation through the membrane can also be based on electrical charge of the membrane – ions of the same charge as the membrane are excluded, and the ions of the opposite charge permeate through the membrane. (Baker 2012; Seader et al. 2011)

3.1 Ultrafiltration

Ultrafiltration (UF) is a pressure-driven filtration process. The pore size distribution of ultrafiltration membranes is typically within the range of 1-100 nm, and the separation is mainly based on size-exclusion, as the particles that are larger than the pores of the membrane, are retained. However, also the shape of the molecules influences the separation result. Ultrafiltration membranes are effective in the removal of macromolecules, colloids, suspended solids, and organic molecules. The operating pressure of ultrafiltration processes varies between 200 – 1000 kPa. (Purkait et al. 2018)

Common membrane materials for ultrafiltration are organic polymers, e.g., polypropylene or polysulphone, or ceramic materials. Polymeric membranes are low-cost, lightweight, and thin – however, the tolerance for oxidants or rough process conditions is typically poor. Ceramic membrane materials can withstand wide ranges of temperature, pH and pressure, but the production costs are high. (Speth et al. 2005)

The separation performance of ultrafiltration membranes is typically portrayed by molecular weight cut off (MWCO) -rating. The MWCO-value of a membrane is defined as the molecular weight that is 90 % rejected by the membrane and it is measured by filtrating particles with known molecular weights (Purkait et al. 2018). However, the

molecular weight of is not the best indicator of the actual size or shape of a molecule. Linear molecules permeate through pores more easily than globular molecules of the same molecular weight. The shape of the molecule is affected by the process and feed conditions: For example, pH, temperature, and ionic strength. (Cheryan 1986)

Ultrafiltration has a wide variety of industrialized applications. In food processing, ultrafiltration can be applied in production of dairy products, beverages, and edible oils. However, the most common industrial application for ultrafiltration is wastewater treatment, particularly separating solid substances from water (De Andrade et al. 2017). The separation of particulates from water is based on sieving mechanism and the pore size distribution of the membrane. The removal of dissolved substances from water may require pre-treatment, such as addition of coagulants to transform the species to particulate form. Ultrafiltration membranes are especially effective in reducing the turbidity, colour, and microbial content of water (Speth et al. 2005). Ultrafiltration membranes can achieve almost complete removals of turbidity (>99 %) and colour (>97 %) of wastewaters (Barredo-Damas et al. 2011).

Ultrafiltration can also be applied to reduction of total organic carbon (TOC): In a study by Domany et al. (2002), humic substance rejections of ultrafiltration membranes were up to 90 % for model solutions and slightly lower (62-69 %) for natural well water. However, the efficiency of ultrafiltration membranes in removal of dissolved organic content without pre-treatments is significantly lower than if a pre-treatment step, such as flocculation, is applied together with ultrafiltration (Goren et al. 2008; Zhang et al. 2006). Another possibility for utilization of ultrafiltration in removal of organic matter is combining ultrafiltration with conventional water purification processes, such as activated sludge process: Ultrafiltration is can effectively reduce the suspended solids content of wastewater, which enables the separate processing of the particulate-rich sludge and the water containing soluble organic matter (Nascimento et al. 2017).

A major drawback for most membrane separation processes – especially for processes based on sieving mechanism - is the fouling of the membranes and an effect called concentration polarization. Fouling and concentration polarization are contributors to flux decline, as the accumulation of particles or generation of a gel layer or cake increases the resistance of the membrane system, limiting the flux. (Sablani et al. 2001; Singh 2015)

Fouling depends mainly on the properties of the feed fluid and the membrane, and the conditions of the filtration process. For many organic foulants, i.e., humic substances, the ionic strength and pH of the solution are connected to severity of fouling. High fluxes and high trans-membrane pressures often lead to rapid fouling (Zhou et al. 2015; Sutzkover-Gutman et al. 2010). Membrane fouling occurs mainly via two mechanisms: Macrosolute or particle adsorption, which is usually irreversible as the foulants adsorb and attach inside pores and block them, or macrosolute or particle deposition, which manifests as cake formation and accumulation of rejected particles on the surface of the membrane (Kumar et al. 2015). In addition to the components of the feed, fouling can be caused by biological organisms, such as algae or bacteria (Purkait et al. 2018; Gao et al. 2011).

Concentration polarization is a phenomenon which is caused by the increasing solute concentration on the feed side of the membrane. As the concentration of feed increases, the particulates accumulate near the membrane surface and form a gel-like layer on the surface of the membrane. The gel layer increases resistance for the permeating liquid, resulting in lower membrane performance. (Scott 1996)

Membrane fouling can be controlled by pre-treating the feed to decrease the concentration of the foulants or transform the foulants into a form that is easily rejected by the membrane. Typical pre-treatment processes for fouling control are coagulation, pre-oxidation, and adsorption. Fouling control can also be implemented through process conditions and operation mode: Backwashing can be used to sweep away the particulates deposited on the membrane surface and inside the pores, and the cake formation on the membrane surface can be controlled by air scouring, in which the surface of the membrane is scraped with pressurized air. Backwashing also mitigates the effect of concentration polarization, as the direction of the fluid flow changes and forces the gel layer to degrade (Gao et al. 2011)

3.2 Alkali-activated materials in membranes

The low raw material costs, lower CO_2 emissions and mild preparation conditions of alkali-activated materials make them a desirable alternative for conventional inorganic membranes. The wide variety of aluminosilicate sources provides flexibility and variety

in terms of adsorptive capacity and textural and mechanical properties of the geopolymer materials and enables the tailoring of the geopolymer properties for a specific use (Della Rocca et al. 2020). In addition to applications in water purification, geopolymer membranes have potential applications in air purification, for example in removal of exhaust particulate matter (Zhang et al. 2021).

Geopolymer membranes have been successfully applied to the removal of solid particles and turbidity from aqueous solution. Metakaolin-based geopolymer membranes have achieved 100 % rejection rate towards aluminium oxide particles (D_{50}=60.28 nm) (Xu et al. 2015), and almost complete (>99.6 %) turbidity and suspended solids removal rates have also been reached in the purification of green liquor from pulp production (Xu et al. 2019). Metakaolin-based geopolymer membranes have also shown potential for the removal of heavy metal ions (Ni^{2+}) from wastewaters (Ge et al. 2015).

Attempts have been made to improve the porosity and properties of geopolymer membranes. The porosity of geopolymers can be manipulated by adding hydrogen peroxide or other foaming agents to the geopolymer paste – however, higher porosity leads to lower mechanical strength. The mechanical strength and the open porosity of highly porous geopolymers can be altered by addition of surfactants, such as egg white. (Bai et al. 2017; Daud et al. 2021)

Composite materials offer possibilities for the improvement of thermal, mechanical, and chemical properties of geopolymer membranes. The defects, voids, and channels of crystalline materials, i.e., zeolites, contribute to the total porosity of the composite material, improving the separation performance and flux (Shao et al. 2020). Zeolite-geopolymer composites are typically obtained by processing the geopolymer hydrothermally. Hydrothermal treatment affects the evolution of the solid, causing conversion of geopolymer gel into zeolite crystals on the surface of the geopolymer (Yan et al. 2021; Azarshab et al. 2016).

He et al. (2020) prepared a composite membrane material from circulating fluidized bed fly ash by treating the geopolymer membrane hydrothermally in an autoclave. The prepared composite membrane was then tested for the separation of hexavalent chromium from aqueous solution. The zeolite-geopolymer composite showed excellent rejection (84.45 %) of hexavalent chromium. Shao et al. (2020) formed a zeolite-geopolymer

composite material based on fly ash geopolymer and converted the geopolymer partially to zeolite with a 16-hour hydrothermal treatment. The membrane was applied to removal of organic pollutants, such as organic dyes and tetracyclines, and rejection rates over 95 % were achieved.

Zeolite-geopolymer composites can also be produced without hydrothermal treatment through the geopolymerization route. Generally, the amount of zeolite increases with the curing temperature or by prolonging the curing time (Pimraksa et al. 2020). Subaer et al. (2020) prepared alkali-activated zeolite-geopolymer composite pervaporation membranes from laterite soil by curing the geopolymer in 70°C for two hours, and in open air for 24 hours before demoulding. Prepared membranes were used in water-ethanol purification. However, the selectivity of the membranes towards ethanol turned out to be low.

In the present study, geopolymer membranes are prepared from metakaolin and blast furnace slag and cured in room temperature. The effect of hydrothermal and thermal treatments on the membrane materials – i.e., zeolite formation – is studied with X-ray diffraction and porosity analyses.

4 MATERIALS AND METHODS

4.1 Preparation of geopolymer membranes

4.1.1 Alkali-activator solution

An alkali activator was prepared by mixing 106.4 g of sodium hydroxide pellets (VWR Chemicals, ≥98 %, GPR RECTAPUR®) with 709.8 g sodium silicate solution (7,5 – 8,5 % Na_2O; 25.5 – 28.5 % SiO_2, Supelco®) in a plastic bottle. The solution was left to stir on a magnetic stirrer for 24 hours.

4.1.2 Preparation of membranes

Three different types of membrane materials were prepared. The main difference was the calcium content of the material: Low-calcium -material was based on metakaolin, medium-calcium material was prepared with metakaolin (Metamax, BASF) and ground-granulated blast furnace slag (Finnsementti), and high-calcium material was based on blast furnace slag. The mix design for the materials is presented in Table 2.

Table 2. Mix design for membrane materials.

	Low-calcium material: Metakaolin	Medium-calcium material: Metakaolin + blast furnace slag	High-calcium material: Blast furnace slag
Alkali activator	57.7 g	37.6 g	17.4 g
Metakaolin	42.3 g	21.2 g	
Blast furnace slag		37.1 g	74.1 g
Deionized water		4.2 g	8.5 g

After initial experiments of pH neutralization, it became apparent that the high-calcium material was extremely brittle and sensitive to acid treatment and drying, and it was left out of the experiments.

Steel petri-dishes from Bochem with a diameter of 75 mm were used as moulds. A small hole (1 – 2 mm) was drilled to the bottom of the moulds and sealed with tape during casting and curing. The edges and bottom of the moulds were coated with clear packing

tape to prevent air escaping from the edges during demoulding, and thin layer of oil was applied. The moulds are shown in Figure 1.

Figure 1. Moulds ready for use.

The ingredients were mixed with a steel spoon in steel mixing cup to form a paste, and the paste was stirred with IKA Eurostar 20 high speed vertical stirrer at 3000 rpm for five minutes. At the halfway of the stirring, the stirrer was stopped, and the edges and corners of the mixing cup were scraped with a steel spoon to ensure that no material was left unmixed.

The paste was casted to the moulds and air bubbles were removed by vibrating the moulds on Prolab 2 Vortex Genie shaker on full speed. The lids were closed, and the moulds were placed to plastic bag and left to cure in room temperature for 24 hours. Demoulding was done by blowing pressurized air (300 – 400 kPa) through the hole in the bottom of the moulds, and the samples popped out. The preparation process is presented in Figure 2.

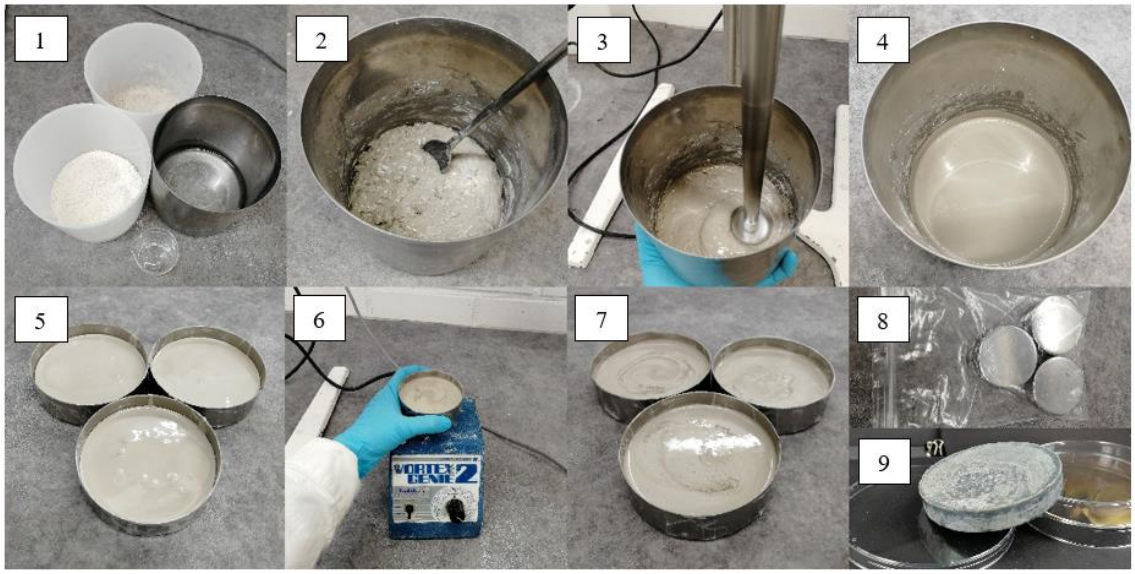

Figure 2. Preparation process.

After demoulding, the membranes were ground to thickness of 3-3.2 mm with rotary polisher (Buehler Metaser Motopol 12) using aluminium oxide-based abrasive papers P60 and P120. After the goal thickness was achieved, the membranes were polished with P240 abrasive paper. Thin, polished membranes (Figures 3 & 4) were stored wrapped in plastic inside plastic petri-dishes to prevent the moisture from evaporating.

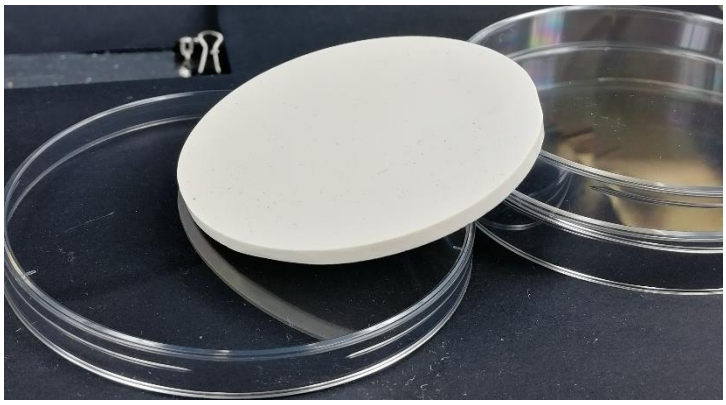

Figure 3. Low-calcium membrane after grinding and polishing.

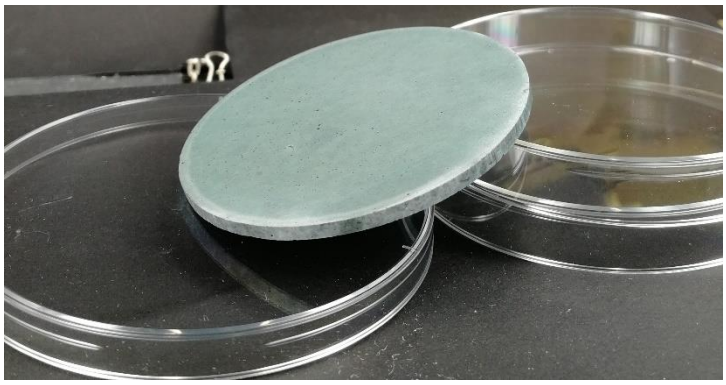

Figure 4. Medium-calcium membrane after grinding and polishing.

4.1.3 Thermal and hydrothermal treatment

Three types of thermal treatment were used for the samples. The samples subjected to thermal treatment were later characterized with BET, BJH and XRD to study the effects of thermal and hydrothermal treatments.

One sample of each material were placed in a furnace, and the furnace was heated to 700°C with a heating rate of 2°C/min. The samples were kept in 700°C for one hour. The goal of this treatment was to convert the geopolymers to high-temperature ceramics. The samples after 700°C treatment are shown in Figure 5.

Figure 5. Low- (left) and medium- (right) calcium geopolymers after heat treatment in 700°C.

One sample of each material were placed in a furnace that was heated to 300℃ with a heating rate of 2℃/min, and the samples were kept in the furnace for one hour. The goal of treatment in 300℃ was to finalize the geopolymerization reactions. Samples after 300℃ treatment are shown in Figure 6.

Figure 6. Low (left) and medium- (right) calcium geopolymers after treatment in 300℃.

In hydrothermal treatment, one sample of each material was placed in a 1000 mL decanter filled with 90℃ water for 15 hours. The purpose of the hydrothermal treatment was to convert the geopolymers into zeolite. Samples, that have undergone hydrothermal treatment, are shown in Figure 7.

Figure 7. Hydrothermally aged samples: Low- (left) and medium-calcium (right).

4.2 Characterization methods

4.2.1 BET / BJH

Specific surface area and pore size are key figures in membrane characterization. Brunaurer-Emmett-Teller (BET)-isotherm and Barrett-Joyner-Halenda (BJH)- method are based on adsorption and desorption of nitrogen gas onto porous solids. The analyses were performed with Mictomeritics ASAP 2020-system shown in Figure 8. The samples were degassed in 70°C before porosity measurements. The purpose of degassing was mainly to remove any adsorbed species, such as water, from the samples.

Figure 8. Mictomeritics ASAP 2020.

BET- and BJH-isotherms were measured for the base material used in membranes and for the thermally and hydrothermally treated samples. All samples were ground to fine

powder with Retsch vibratory disk mill by placing the samples in the grinder and grinding for 60 seconds at the speed of 1500 rpm.

4.2.2 X-ray powder diffraction

The mineralogy of the membrane materials is examined by X-ray powder diffraction (XRD). In XRD, the sample is subjected to X-rays in different angles, and the presence of crystalline minerals is determined, and the minerals are identified, based on the scattering of x-rays. The scattering angles are mathematically converted to a form that can be compared to known reference patterns of minerals. Sharp peaks in the XRD curve indicate crystals, whereas a broad maximum indicates amorphous structure. (Cullity et al. 2001)

The applied XRD system was Rigaku SmartLab 9 kW. Analysed samples were ground to fine powder similarly to the BET and BJH samples.

4.2.3 Zeta-potential

Electrical charge of membranes can be exploited in reducing fouling effects and increasing membrane performance and retention of charged species (Zydney 2016). Most membranes are naturally neutral or negatively charged due to the materials and preparation methods used in membrane fabrication. Membrane surface charge is often expressed as zeta potential and the charge of the membrane has a great effect on membrane performance, as a charged membrane will repel similarly charged species, which improves retention and reduces concentration polarization (Williams 2016). In the present study, zeta potential of the prepared membrane materials was determined to gain understanding on the aptitude of geopolymer membranes to purification of wastewaters.

Zeta potential was measured from solutions that contained 0.1 weight- % of the ground geopolymer powder in deionized water. Before preparing the solutions, the geopolymer powders were neutralized by rinsing with 0.1 M acetic acid and deionized water on filter paper until the pH of the water was 7 – 7.5. After neutralization, the neutralized powder was mixed with deionized water. The zeta potential measurements were taken with Malvern Zetasizer at the Oulu Mining School research centre.

4.2.4 Scanning electron microscopy

In scanning electron microscopy (SEM), small samples are placed in a vacuum chamber and irradiated with an electron beam. The interactions between the sample and the electron beam produce electron backscatter, characteristic X-rays, and secondary electrons, which are detected by the SEM detectors, and converted to an image. (Reed 1996)

The microstructure of the samples was studied with scanning electron microscopy (SEM) using Zeiss Ultra Plus field emission scanning electron microscope. Small fragments (<10mm x 10 mm) of the polished membranes were coated with carbon before the analysis.

The elemental composition and structural analyses were performed with electron backscatter diffraction-camera and energy-dispersive X-ray spectroscopy-elemental analysis.

4.2.5 Shrinkage and change in mass

The shrinkage and change in mass of the prepared geopolymer materials was measured by casting the paste into 40 mm x 40 mm x 160 mm moulds and inserting steel nuts in both ends of the moulds. The samples were cured in room temperature for 24 hours before demoulding.

After demoulding, the samples were stored in room temperature and one of each sample was sealed in a plastic zip-lock bag. The change in the length and mass of the samples was followed daily for the first week after demoulding, and then every other day until 28 days after demoulding.

4.2.6 Flexural and compressive strength

Samples for flexure and compressive strength tests were prepared by casting three 20 mm x 20 mm x 80 mm samples of each material. After curing the samples in room temperature for 24 hours, the samples were sealed in a plastic zip-lock bag and left to set in room temperature for 28 days.

The flexure and compressive strength tests were done with Zwick 100kN universal testing machine. The flexural strength of the samples was tested with the three-point bend test. In three-point bend test, the sample rests on two supports, and a concentrated load is subjected at the centre of the sample until the sample fractures. The flexural strength of the samples was calculated based on Equation 2.

$$\sigma_f = \frac{3FL}{2bw^2} \quad (2)$$

In equation 2, F stands for the load at the fracture point [N], L for the support span [mm], and w and d for the width [mm] and depth [mm] of the sample. Compressive strength of the samples was determined similarly by measuring the load [N] required to shatter the samples and dividing the load with the area of under stress. A small piece of metal with area of 400 mm^2 was placed on the samples in compression strength tests to standardize the area under stress.

Same samples were used in both flexural and compression strength tests: First, flexural strength test was done for the 20 mm x 20 mm x 80 mm samples, and the halves of the samples were collected and used in the compressive strength tests. As the samples were irregular in size and shape after flexural strength tests, a 20 mm x 20 mm rectangular piece of metal was placed on the samples in the compressive strength tests to provide constant area under stress.

4.3 Filtration experiments

All filtration experiments were performed with CM-CELFA's laboratory scale membrane unit P-28. The membrane unit consists of a membrane cell, which uses a flat sheet membrane with a diameter of 75mm, heated feed tank, pump, pressure indicators and pressure control and discharge valves for permeate and retentate. The membrane unit is shown in Figure 9.

Figure 9. P-28 Membrane unit

The temperature and pressure were fixed to 25°C and 200 kPa in all experiments except the water flux experiments. Temperature was controlled by a water-circulating heating system and the operating pressure was maintained by nitrogen gas.

4.3.1 Water flux

Water permeation of the prepared membranes was investigated by filtrating pure, deionized water in different temperatures (20 – 60°C) at constant pressure and in different pressure conditions (200 – 1000 kPa) at constant temperature. The volume of the water permeating through the membrane during a timeframe (generally 2 – 10 minutes) was collected and measured, and the flux was calculated as following equation:

$$J = \frac{V}{A * \Delta t} \quad (3)$$

Where J is the flux (L/m^2h^{-1}) through the membrane, V is the volume of the collected permeate, Δt is the sampling time (h) and A is the membrane area (m^2). As the diameter of the membranes is 75 mm, the area of a membrane is 0.004418 m^2.

4.3.2 pH-neutralization

As the pH of alkali-activated materials is high due to hydroxyl anions (OH^-) remaining in the pore solution, neutralization is required to improve the membrane performance for certain purposes.

Membranes were neutralized by filtrating 0.1 M acetic acid solution (Acetic acid 100 % glacial, Supelco®, diluted to deionized water). After filtrating acetic acid solution, the filtration apparatus was cleaned by filtrating pure, deionized water in two 15-minute batches. Then, one final round of filtration with pure, deionized water was done, and the pH of the permeate was measured with Hach HQ10d meter equipped with IntelliCal pH electrode. The acetic acid filtration, cleaning and measuring sequence was repeated until the pH of the permeate reached 7 – 8.5.

4.3.3 Humic acid solution filtration

The separation performance of the prepared membranes was tested by filtrating 20 mg/L humic acid (technical, Sigma-Aldrich, diluted to deionized water) solution in 25°C and 200 kPa pressure.

The feed tank of the membrane unit was filled with the solution and 2 mL samples of permeate and retentate were collected continuously until the membrane fouled and flux declined. The samples were diluted with deionized water by ratio 1:10.

The humic acid concentration was estimated with UV-VIS spectrophotometry. Dissolved organic carbon (DOC) measurements were analysed by an external laboratory, Eurofins, to confirm the results.

4.3.4 Ammonium ion solution filtration

In ammonium ion filtration experiments, a 50 mg/L ammonium ion solution was prepared by mixing 50 mL of 1000 mg/L ammonium ion solution (Sigma-Aldrich, ammonium ion

solution for ISE) to 1 L of deionized water. 500 mL of the solution was used to fill the feed tank of the membrane unit. The filtrations were performed in 25°C, 200 kPa and 2 mL samples of permeate and retentate were collected continuously during operation. The measuring time varied depending on the permeation rate in each experiment.

All collected samples, including a sample of the feed solution, were diluted with deionized water with 1:25 ratio to obtain 25 mL samples. One ionic strength adjustor pillow (Hach) was added to each sample and the ammonium ion concentration of the samples was measured with Hach HQ4100 meter equipped with an IntelliCal ammonium ion selective electrode.

5 RESULTS AND DISCUSSION

The experimental phase was divided to two parts: The first part focused on characterization of the membrane materials, and the goal of this part was to determine the chemical, physical and mechanical properties of the prepared membranes. Specific surface area and pore properties were studied with BET-isotherm and BJH-method using the equipment and expertise of Environmental and chemical engineering research unit. Mineralogy and microstructure of the membranes was studied with SEM and XRD at the centre of material analysis. Zeta-potential testing was carried out at the Oulu Mining School research centre and strength testing in the laboratory of Materials and mechanical engineering unit.

In the second part, a series of filtration experiments was conducted to evaluate the separation performance of the prepared membranes. The filtration experiments were carried out at with CM-CELFA P-28 membrane unit at the Environmental and chemical engineering research unit laboratory. All samples were analysed at the Fibre and particle engineering unit. Humic acid concentration of the samples was measured with VWR Double beam UV-VIS spectrophotometer (UV-6300PC) and samples from ammonium ion solution filtrations were analysed with portable Hach HQ4100 multi meter and an ammonium selective electrode (Hach Intellical ISENH4181).

5.1 Characterization of the membrane materials

5.1.1 Porosity

The porosity of the membrane materials was studied by Brunauer-Emmet-Teller-isotherm (BET) and Barret-Joyner-Halenda-method (BJH) with nitrogen gas. Unpolished samples were ground to fine powder for the analysis. As hydrothermal treatment was done by submerging the samples in water, hydrothermally treated samples were dried in 60°C oven for two days to reduce the moisture content of the samples before analysis.

Results from BET and BJH are shown in Table 3.

Table 3. BET and BJH results.

Sample	Micropore area (m2/g)	Micropore volume (cm3/g)	Average pore diameter [nm]	Total BET surface area
Low-calcium	3.74	0.0018	12.06	40.69
Low-calcium, hydrothermal treatment 90°C	1.69	0.0008	10.78	25.05
Low-calcium, 300°C	1.03	0.0005	13.17	15.09
Low-calcium, 700°C	0.68	0.003	14.79	12.73
Medium-calcium	*	*	5.27	48.47
Medium-calcium, 90°C	2.12	0.0009	9.55	28.49
Medium-calcium, 300°C	1.03	0.0005	13.73	13.42
Medium-calcium, 700°C	0.57	0.0003	27.42	1.78
		*micropore area is not reported because the micropore volume is negative		

The pore volume and BET surface area of low-calcium material decreased consistently as the temperature of thermal treatment increased. A decline in BET surface area and pore volume of metakaolin-based geopolymer after thermal treatment has also been observed by Duxson et al. (2007). Decline in the pore volume and BET surface area shows that densification occurred during thermal treatment, and the samples that were treated in high temperatures (300°C & 700°C) lost circa 10 % of their diameter in the treatments.

The micropore area of medium-calcium samples was not calculated as the micropore volume was negative. This may be due to extremely small pore size of the sample, or the porosity of the material being too low to measure. The pore volume of medium-calcium membrane without thermal treatment was negative, and the average pore diameter was 5.26 nm. Average pore diameter of medium-calcium material treated in 700°C was 27.42 nm, which is nearly twice as high as the average pore diameter of the low-calcium material treated in the same temperature (14,79 nm).

The measured BET surface areas are in the same range as obtained BET surface areas for similar geopolymers in literature. Values in the range of 2.8 – 39.6 m^2g^{-1} (Ge et al. 2015), 42.5 – 76.9 m^2g^{-1} (Zhang et al. 2021), 6.5 – 97.8 m^2g^{-1} (He et al. 2013), and 13.3 – 30.1 m^2g^{-1} (He et al. 2020), inter alia, have been reported.

5.1.2 Structure and elemental composition by SEM

As the membranes were ground and polished by hand, some concerns aboout the quality and uniformity of the membrane surface were raised. An optical microscope was used to study the surface of the membranes. Two samples of each material from different preparation batches were examined to see if the storage time had any effect on the membrane surface, as the membranes seemed to fracture and break if they were stored for long periods of time withoud plastic wrapping and addition of water.

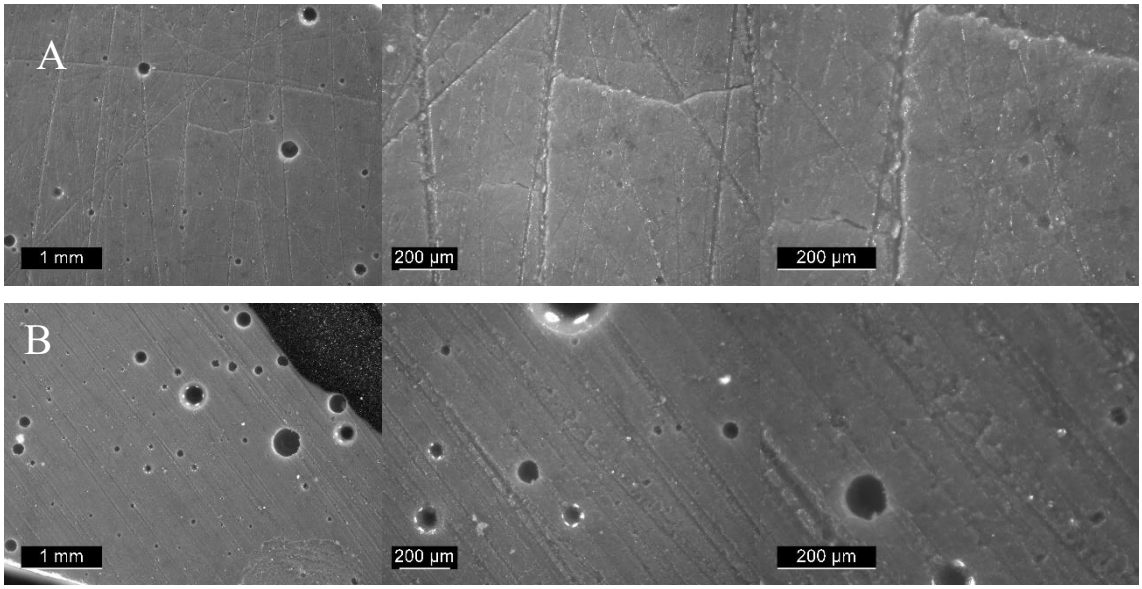

Figure 10. Low-calcium-membrane: (A) seven days after casting and (B) 28 days after casting

For low-calcium membranes, the concerns about the uniformity and quality of grinding were proven right: Some clear abrasion marks were observed on the surface of one membrane (Figure 10). Grinding and polishing times were not standardized, and the result of polishing was not monitored with nothing but bare eye during the grinding process. Similar abrasion marks can be observed in the medium-calcium membranes but to less extent: Slight abrasion marks can be seen on the surface of the older membrane, while the younger membrane is smooth. Differences in surface quality could be controlled by standardizing the grinding and polishing time and the force at which the membrane is pressed against the abrasive paper, and by using a finer abrasive paper as the final stage of polishing.

The amount of air bubbles on the membrane surface differs between preparation batches. One of the low-calcium membranes has a considerable amount of large (up to 0.5 mm) air bubbles remaining, and both medium-calcium membranes have several smaller air bubbles, even though the vibration time was standardized. This might be due to differences in casting height, as the 60 second vibration may not be enough to lift the bubbles to the surface of a thicker paste layer. Another factor contributing to the amount of remaining air bubbles is grinding; as neither the grinding time nor pressure was monitored, there remains a possibility that some membranes received more intensive grinding on the top surface than others.

The connection between surface defects, such as abrasion marks or air bubbles, and the membrane performance is twofold. Rougher membrane surface with voids and gaps increases the surface area available for mass transfer, which indicates better membrane performance. However, rough membrane surface area is a major contributor to membrane fouling, as foulants and particles accumulate to the ridges and valleys of the surface. The decline in flux is typically steeper for rougher membranes. (Kumar et al. 2015)

Surprisingly, neither of the 28-day-old membranes show clear signs of fracturing of breaking. The 7-day-old medium-calcium membrane has a small fracture at the upper left corner; however, the analysed piece is a fragment of a membrane that broke during grinding, so the fracture is likely not age-related but rather impact-related.

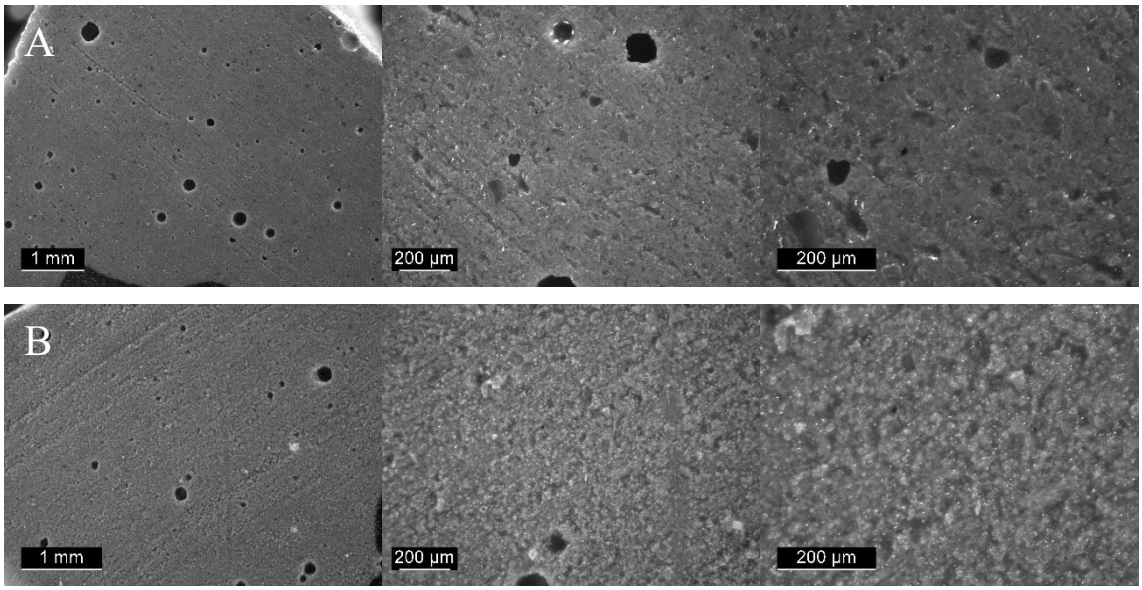

Figure 11. Medium-calcium-membrane: (A) Seven-day-old and (B) 28-day-old.

The surface of the 28-day-old medium-calcium membrane has lighter areas and is a bit rougher than the surface of the 7-day-old medium-calcium membrane (Figure 11). One possible explanation for this could be the formation of sodium or calcium carbonates or other impurities on the surface as the membrane has had longer exposure to air.

The microstructure of the 28-day-old membranes was studied with field emission scanning microscopy (FESEM), with 100 – 10 000 x magnifications. The elemental composition of membranes was analysed with energy-dispersive X-ray spectroscopy-elemental analysis.

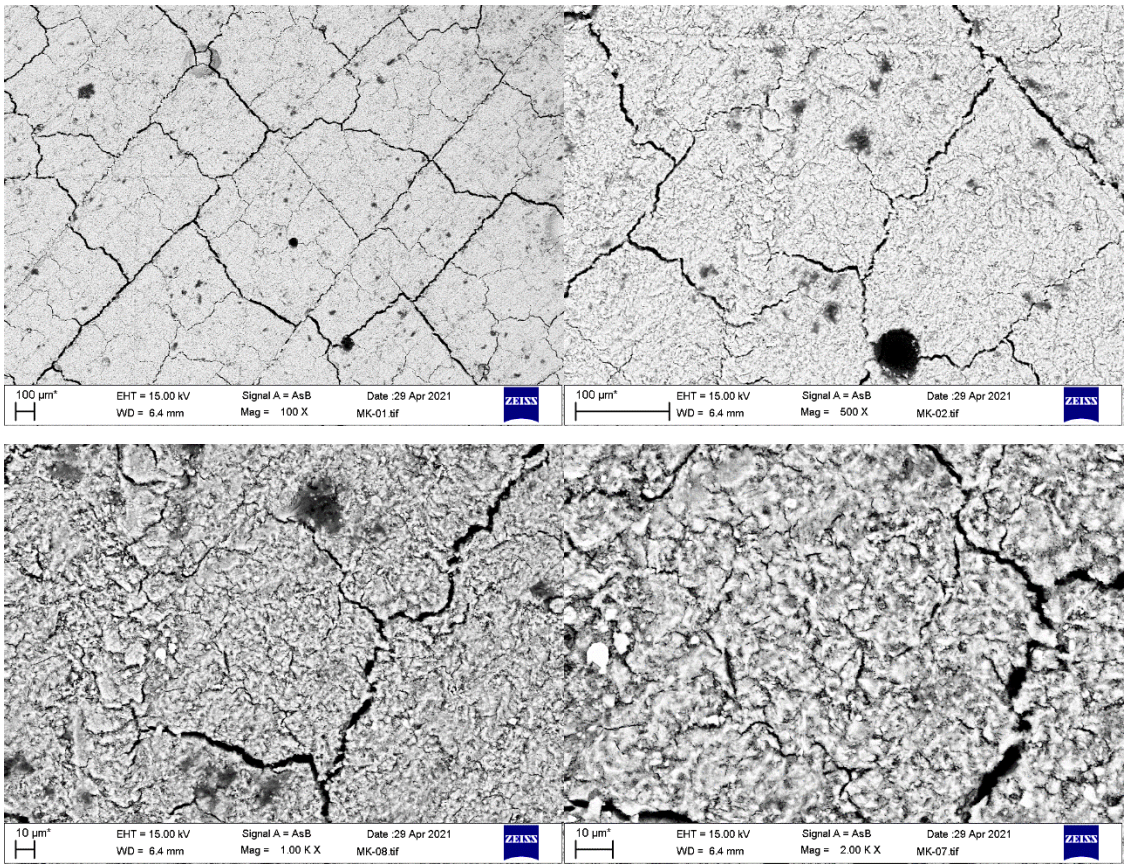

Figure 12. 100 - 2000 x magnifications of low-calcium membrane.

FESEM images (Figures 12 – 15) highlight the roughness of the membrane surfaces. In addition to smaller 50 – 100 µm air bubbles, the 28-day-old low-calcium membrane shows clear, 1 – 5 µm wide fracture lines along the surface. It was observed that rapid drying after grinding resulted in fractures and cracks, and one possible explanation for the fracture lines is the drying of the membrane during storage.

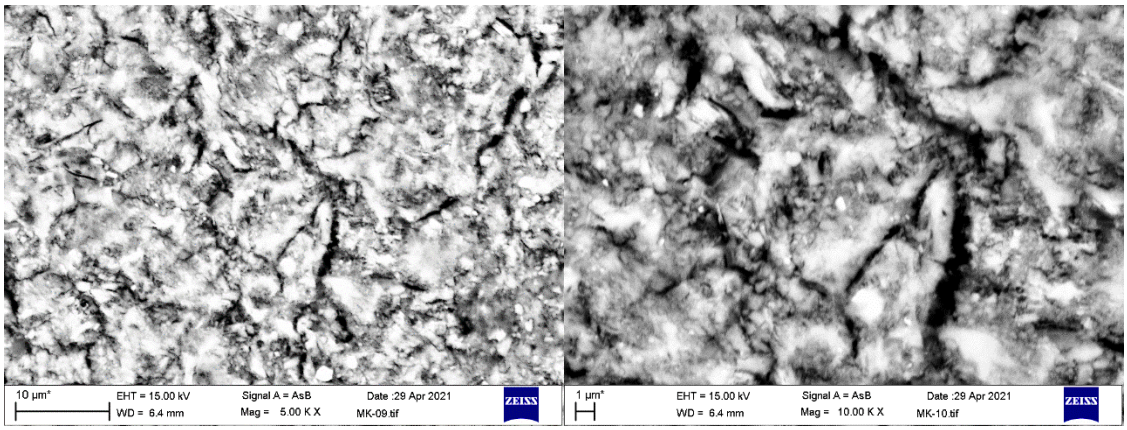

Figure 13. 5000 - 10 000 x magnifications of low-calcium membrane.

The elemental analysis for low-calcium membrane is presented in Table 4. The major components of the low-calcium membrane are silica (25.04 weight- %), oxygen (50.88 weight- %), aluminium (13.98 weight- %) and sodium (7.88 weight- %).

Table 4. Elemental analysis for low-calcium membrane [weight- %].

	O	**Na**	**Al**	**Si**	**P**	**Ca**	**Ti**
Average weight- %	50.88	7.88	13.98	25.04	0.38	0.39	1.89
Max.	54.56	8.83	17.48	28.61	0.50	0.70	15.94
Min.	46.35	6.41	8.09	14.09	0.23	0.23	0.23

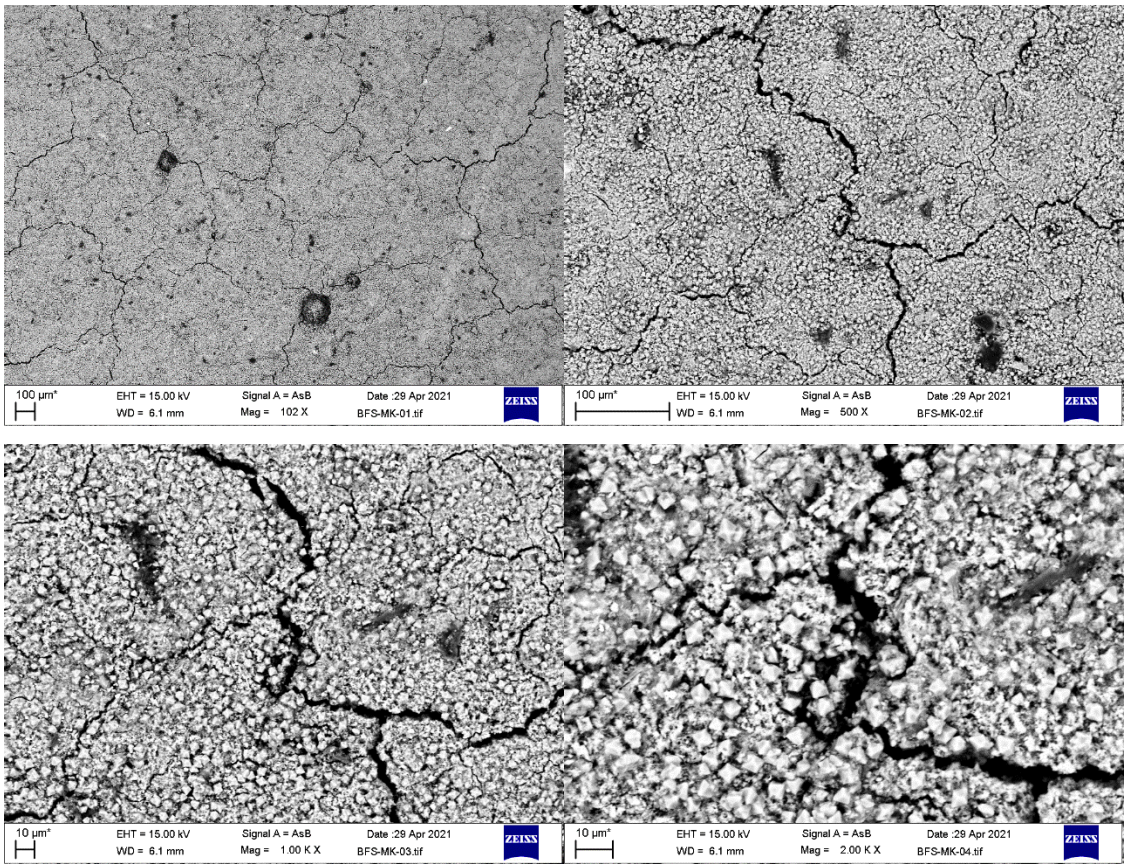

Figure 14. 100 - 2000 x magnifications of medium-calcium membrane.

Larger magnifications (Figure 15) of the medium-calcium membrane reveal deposition of sharp, crystal phases on the surface. The crystals cover a large proportion of the area of the membrane.

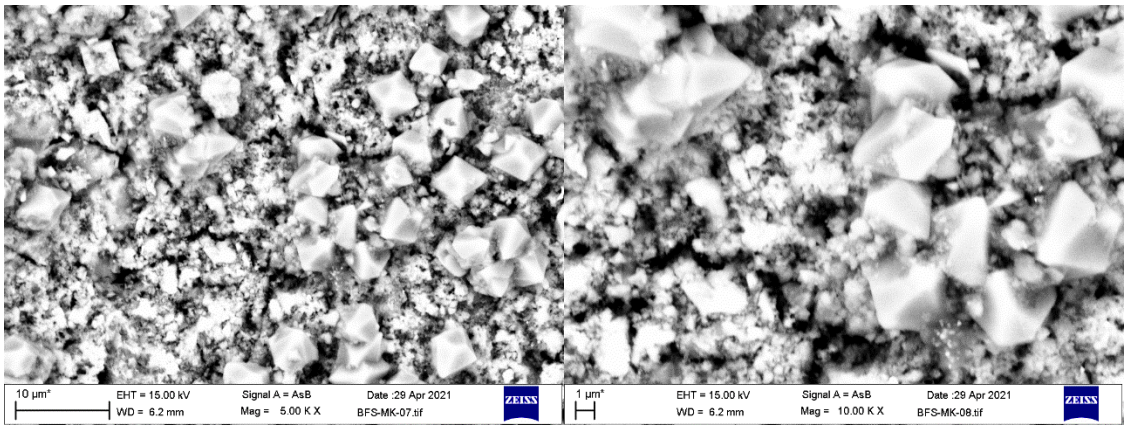

Figure 15. 5000 - 10 000 x magnifications of medium-calcium membrane.

Based on the elemental analysis (Table 5), the crystals are likely calcium derivatives: As discussed earlier on chapter 2.1.1., the average calcium (as CaO) content of blast furnace slag in Finland is up to 42 %, and calcium residues in the membrane may have reacted with the moisture remaining in the membrane and the surrounding air and form calcium carbonate ($CaCO_3$), or less likely, calcium hydroxide ($CaOH_2$). According to the elemental analysis, the average calcium content of medium-calcium membranes was 28.15 weight- %, whereas the average calcium content of low-calcium membranes was only 0.39 weight- %. Calcium hydroxide has been recognized in earlier studies by Cho et al. (2018) and Bella et al. (2020).

The calcium crystals may be one of the reasons for the low fluxes of the medium-calcium membranes, as the solubilities of both calcium hydroxide and calcium carbonate in water are low: The growing crystals clog the pores and limit the flux and the dissolution of the crystals may require acid treatment. Even though the solubility of calcium carbonate increases as temperature decreases and solubility of calcium carbonate, the highly alkaline pH in the filtration system caused by the alkaline membrane likely impairs the solubility (Coto et al. 2012).

Table 5. Elemental analysis for medium-calcium membrane [weight- %].

	O	Na	Mg	Al	Si	P	S	K	Ca	Ti	Fe
Average wt- %	50.28	2.50	1.42	4.97	12.51	0.45	0.55	0.50	28.15	1.18	0.49
Max.	71.38	5.76	3.45	12.28	37.61	0.54	0.97	1.08	48.41	3.29	0.58
Min.	14.74	0.35	0.24	0.29	0.66	0.32	0.28	0.21	8.65	0.26	0.37

5.1.3 Morphology and mineralogy

The purpose of X-ray diffraction analysis was to study the morphology and mineralogy of the materials. In addition to the material used in the membranes, XRD was done for the thermally and hydrothermally treated samples to study the effect of the treatments. Similarly to BET and BJH, a fine powder was prepared for X-ray diffraction by grinding

the samples with vibratory disk mill. The XRD patterns for the samples are shown in Figures 16 – 19.

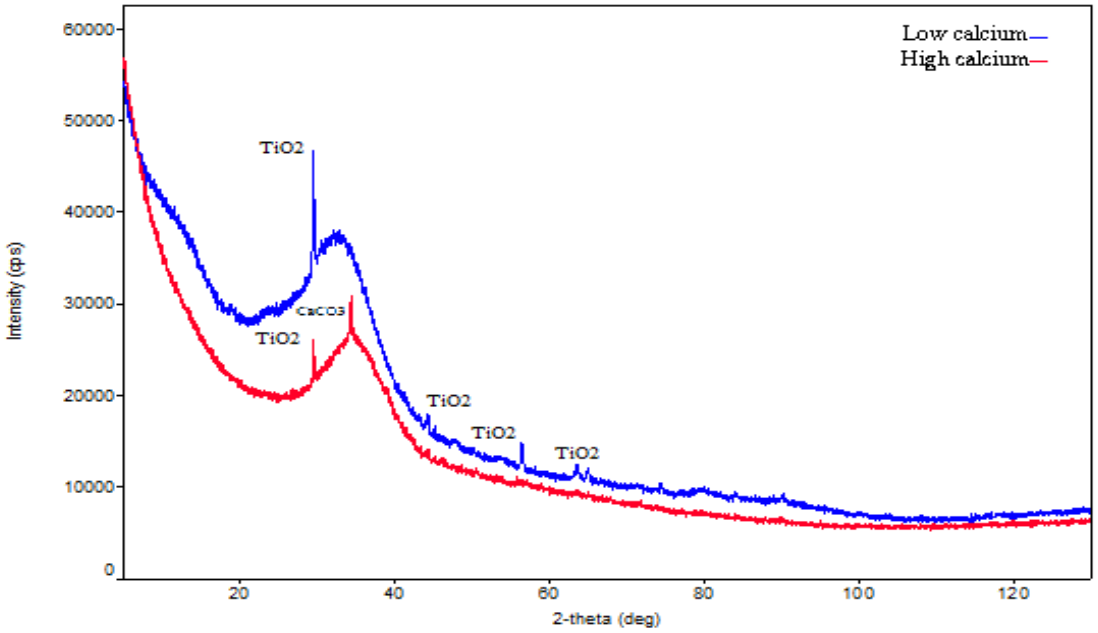

Figure 16. XRD patterns for low-calcium and high-calcium materials.

XRD patterns reveal that all of the analyzed samples are mainly amorphous, and only few intensive peaks indicating crystalline phases exist in the XRD patterns. For the low-calcium material, the only clearly regocnizable crystalline phase is anatase. Anatase is found naturally as a minor constituent in rocks, and it can be synthesized by hydrothermal treatment from titanium bearing rocks in alkaline, neutral or mildy acidic conditions (Deer et al. 2013; Jeantelot et al. 2018). For medium-calcium sample, XRD pattern shows one clear peak and few smaller peaks indicating calcite (calcium carbonate), which is likely a reaction product from reactions between the calcium in blast furnace slag, water, and air.

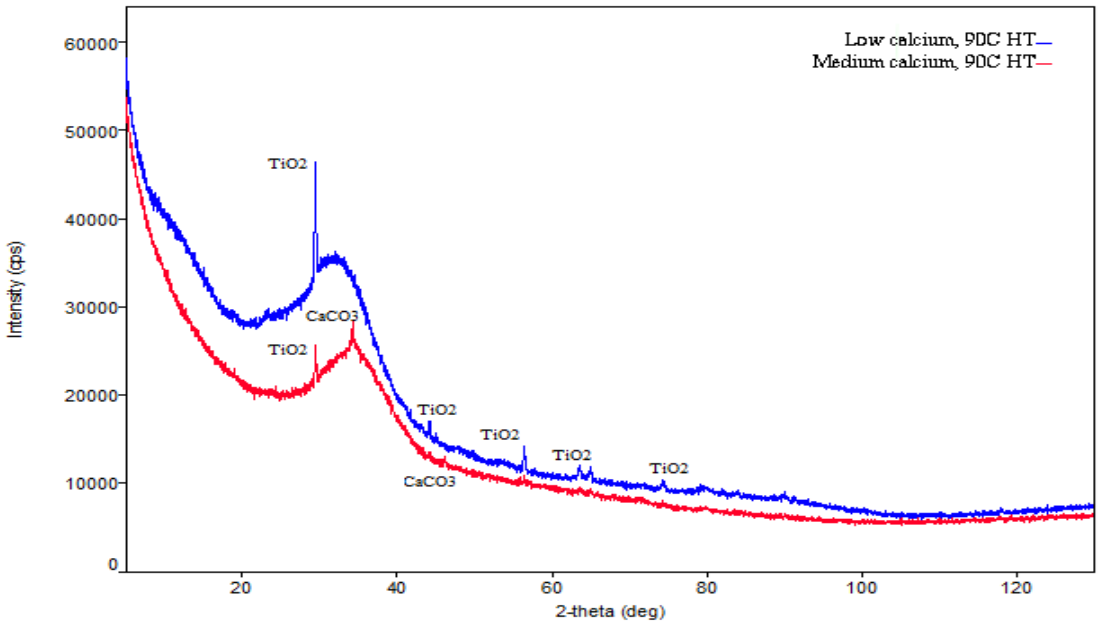

Figure 17. XRD pattern for hydrothermally (90°C) treated samples.

Hydrothermal treatment in 90°C had no notable effect on the crystallinity of the material (Figure 17). The peaks of anatase and calcite are very similar to the peaks in Fig. 10. One possible explanation for the similarity of the hydrothermally treated samples and base samples is the storage time – a technical problem with the XRD equipment delayed the analysis with several weeks, thus prolonging the time the samples were stored and giving more time for zeolite growth in the non-treated samples.

The intensity of the peaks is slightly lower for thermally treated samples (Figures 18 – 19), and the XRD pattern shows a wide bump instead of defined peaks. This indicates that the degree of zeolite formation of geopolymers in high temperatures is low, and the materials are highly amorphous. Similar XRD results showing a small number of low intensity peaks have been presented by Zhang et al. (2021) and Xu et al. (2019), among others. The medium-calcium sample treated in 700°C shows a number of low, sharp peaks of nepheline ($(Na_3K)AlSiO_4$).

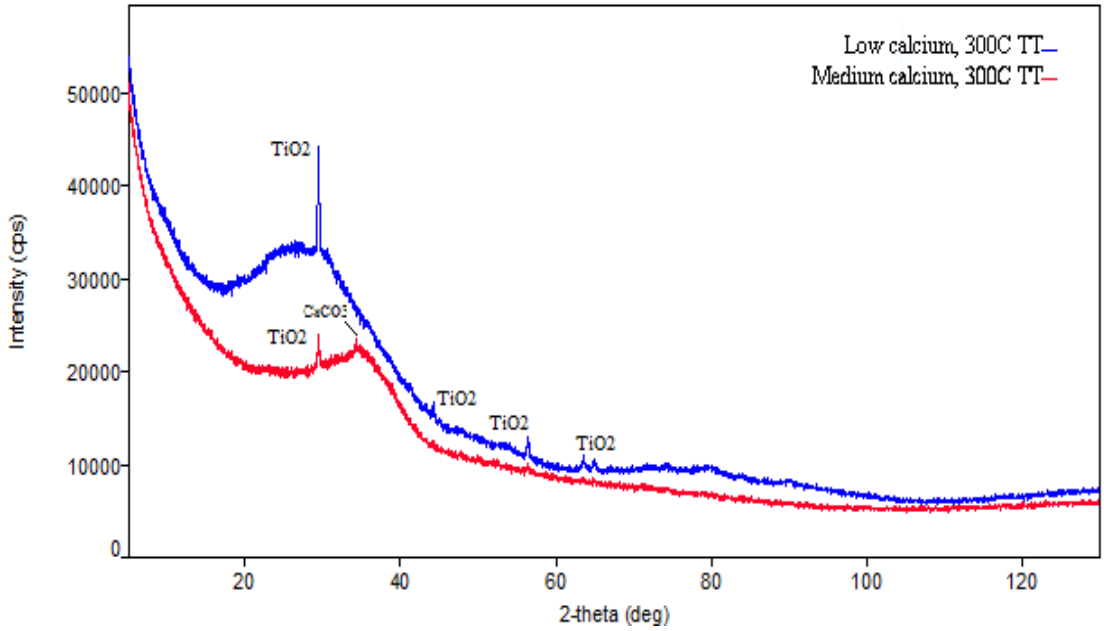

Figure 18. XRD pattern for 300℃ thermally treated samples.

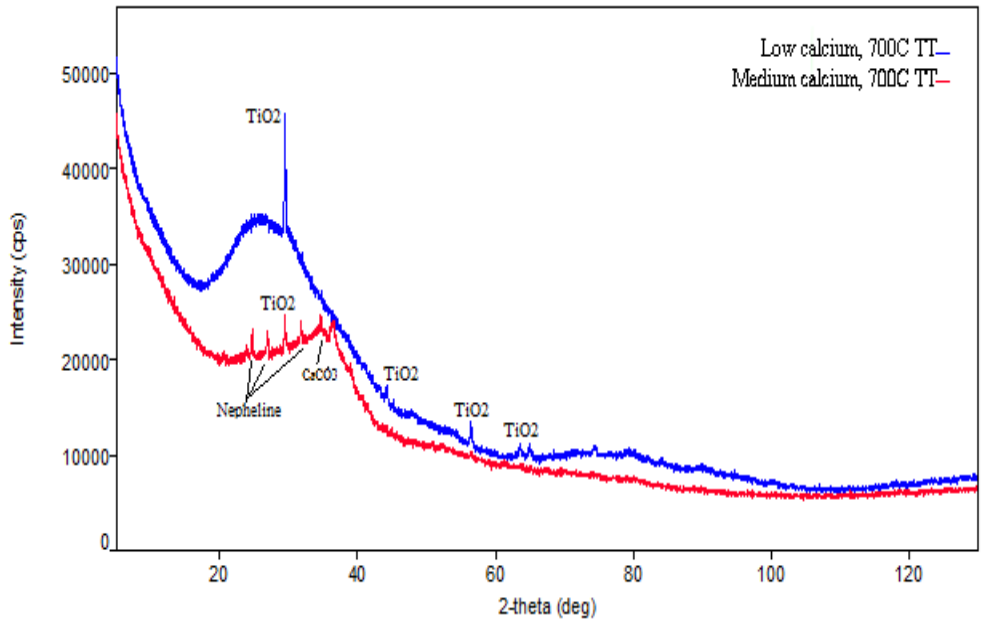

Figure 19. XRD pattern for 700℃ thermally treated materials.

5.1.4 Zeta-potential

The results from zeta-potential measurements are shown in Figures 20 and 21. The average zeta-potential value was -48.52 mV for low-calcium material and -42.06 mV for medium-calcium material. This observation is in line with previous research by Kara et al. (2018): The isoelectric point, in which the solution pH at which the surface charge is zero, is around pH 2 – 4 for metakaolin based geopolymers, and in higher pH values the surface charge of the geopolymer is negative. The negative zeta-potential is probably due to the presence of negatively charged Al-surface sites and/or silanol (Si-OH) groups on the surface.

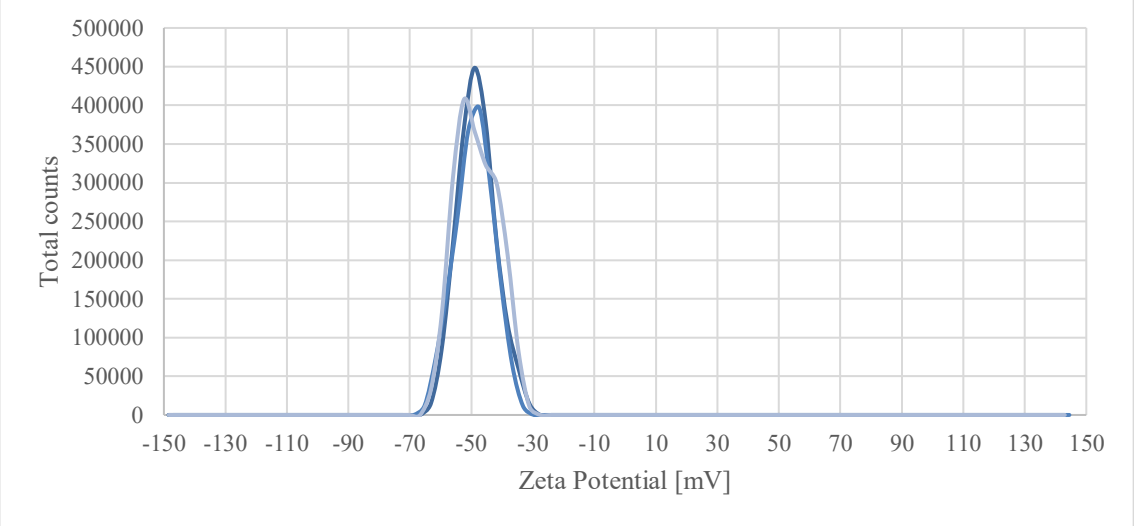

Figure 20. Zeta potential distribution for low-calcium membrane. Measurement was taken three times from the prepared 0.1mg/ L sample.

As the metakaolin content of the geopolymer is relatively high, it was expectable that the zeta potential values would be similar to the low calcium material. Literature did not provide any benchmark zeta potential values for similar geopolymers in same pH conditions; However, the general trend supports the findings: Zeta potential values between -10 – -50 mV have been measured for class F fly ash and blast furnace slag geopolymers (Ghosh et al. 2018; Gunasekara et al. 2015). Negative zeta potential indicates high affinity towards cationic species.

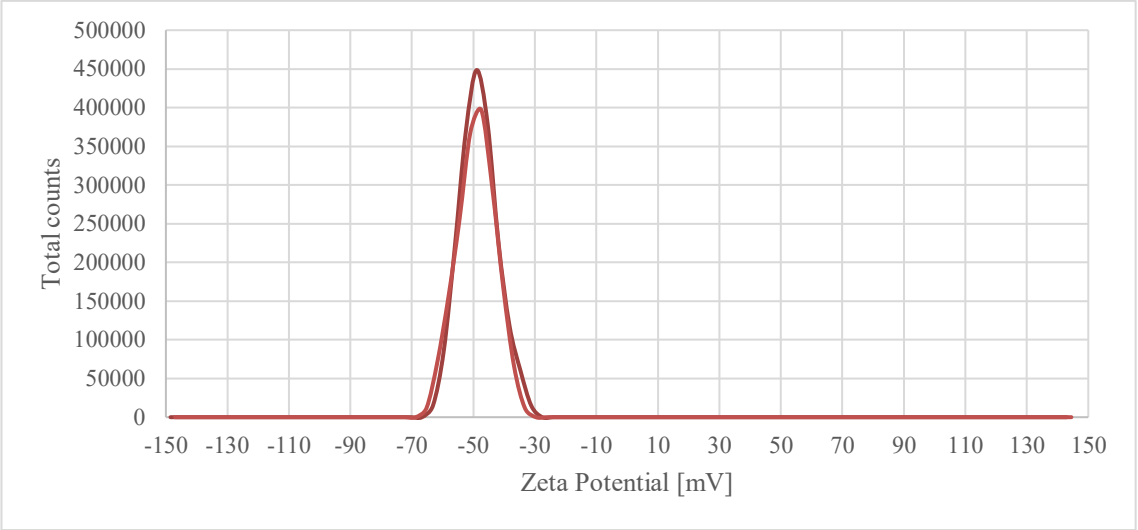

Figure 21. Zeta-potential distribution for medium-calcium membrane. Measurement was repeated twice.

5.1.5 Shrinkage & change in mass

Shrinkage and change in mass of the samples was measured for 30 days after curing. The purpose of the experiment was to determine how exposure to air affects the samples and how much water evaporates from the samples during the timespan. One sample of each material was stored sealed in a plastic bag, and one sample was stored in a cupboard unsealed.

The results from the shrinkage measurements are presented in Figure 22. The length of the samples did not change drastically during the experiment: All samples retained over 99.5 % of their initial length. Some visible cracks appeared on the samples during the experiment, and the cracking of the samples also explains the spikes in the length of the samples: The slope of the curve is smoother for the sealed samples, which had less cracks and fractures, and a few deviant values can be spotted from the curves of the unsealed samples.

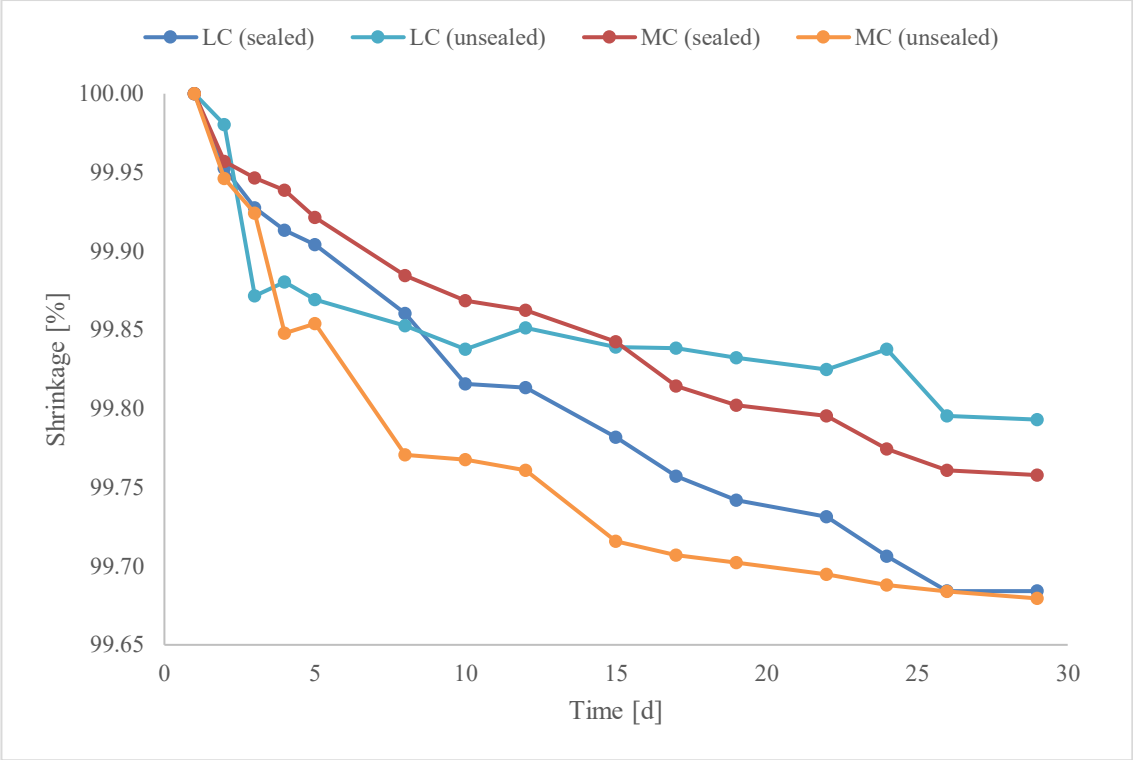

Figure 22. Shrinkage curves (%) for the sealed and unsealed low-calcium (LC) and medium-calcium (MC) samples.

Drying shrinkage of alkali-activated materials is a major concern in some potential applications of the materials, including construction. The reason behind drying shrinkage is mainly the loss of structural water. Generally, industrial slag-based alkali-activated materials have the highest drying shrinkage, and the shrinkage can be controlled to some extent by curing in elevated temperature or high relative humidity, replacing part of the slag with other materials, or by introducing additives or fibres to the paste. (Mastali et al. 2018; Hojati et al. 2019)

In addition to cracking, exposure to air had other observable effects on the samples: The medium-calcium sample, which was greenish at the beginning of the experiment, slowly changed colour, and was almost as pale as the low-calcium sample at the end of the experiment. The greenish colour of blast furnace slag-based materials, and the change of colour from green to almost white has been under particular interest as the colour affects the aesthetics of blast furnace slag-based building materials (Chaouche 2017). The

change in colour of the samples can be observed from Figure 23. Sealed sample has still some of the characteristic greenish colour left, and the unsealed sample has turned pale, almost completely white. Similar fading of colour was also observed in the medium-calcium membranes during long periods storage.

Figure 23. Blast furnace slag samples after 30 days. Unsealed sample on the left, sealed sample on the right.

The samples stored in sealed plastic bags lost less than 2 % of their mass in 30 days (Figure 24), while the low-calcium sample lost nearly 10 % of mass and medium-calcium sample 15 % of mass. The loss of mass is due to the moisture of the samples evaporating: For sealed samples, the plastic limited the rate of evaporation.

Fracturing and cracking of the membranes as they dried after polishing and during storage was an issue in the filtration experiments, and the membranes had to be stored wrapped tightly in plastic and some water had to be added inside the plastic in order to prevent the membranes from breaking. If the membranes were stored completely exposed to air after polishing, the cracks appeared within minutes due to the thinness of the membrane.

Fracturing and evaporation of water could be avoided by storing the membranes in humid environment.

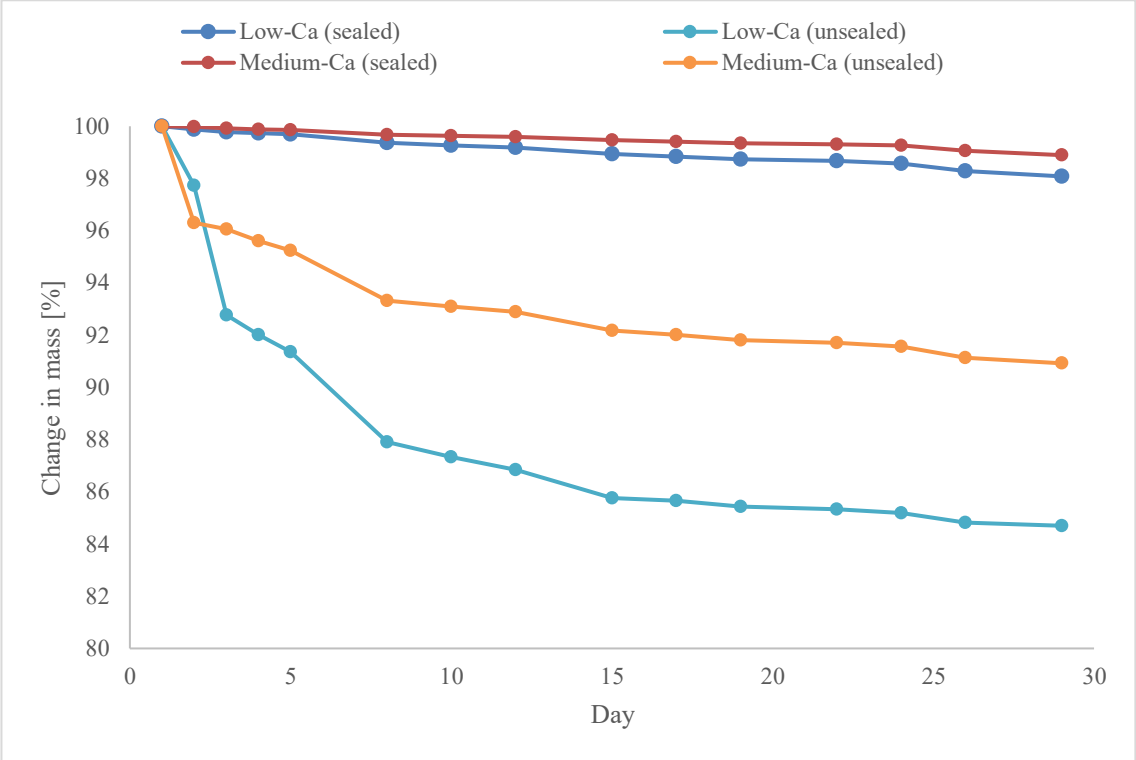

Figure 24. Change in mass in 30 days.

5.1.6 Flexural and compressive strength

Three 20 x 20 x 80 mm samples of both materials were prepared for strength testing: First, the flexural strength test was done for the samples and then the halves of the original samples were used in the compressive strength tests.

The flexural strength test was repeated three times for each material and the mean was calculated. For low-calcium material, the flexural strength varied in the range of 6.15 – 11.12 MPa with a mean value of 8.21 MPa. For medium-calcium samples, the range was from 5.35 – 7.76 MPa, mean value being 6.46 MPa.

Compressive strength test was done six times for each material, by using the halves of the samples from flexural strength tests. Compressive strength of low-calcium samples varied between 33-66 MPa, with an average of 56.30 MPa. For medium-calcium material, the

range was 67-93 MPa and the mean value 78.31 MPa. The compression strength of the membrane materials is significantly higher than the pressures applied in the filtration experiments (0.2 – 1 MPa), which indicates that the breaking of membranes in filtration experiments is unlikely to be related to the operating pressure of the unit.

According to Bakria et al. (2011), there exists a clear relationship between geopolymer curing conditions and the mechanical strength of the materials: Mechanical strength of geopolymers increases with curing temperature and curing time. In terms of compressive strength, the optimal curing temperature is 60°C - in temperatures above that, the mechanical strength decreases. (Chen et al. 2016; Bakria et al. 2011).

5.2 Filtration experiments

5.2.1 Water flux

The water flux results are calculated based on the equation presented in chapter 4.3.1. Each measurement was repeated 2 – 3 times and two membranes of each material was tested to confirm the repeatability of the results. First, initial testing was done to determine the temperature and pressure range, and the lower limit of pressure was set to 200 kPa as there was no flux through the membrane in pressures below that. For temperature testing, the lower limit was set to room temperature and upper limit to 60°C, as the membranes showed signs of breaking in 50 – 60°C and above.

In the first experiment, the temperature was set to room temperature (20°C) and the permeated volume was measured in different pressures (200, 400, 600, 800 and 1000 kPa) by opening the permeate valve for a controlled time (2 – 10 min) and collecting the sample to a small graduated cylinder. The average water fluxes with standard deviation for low-calcium and medium-calcium membranes are presented in Figure 25.

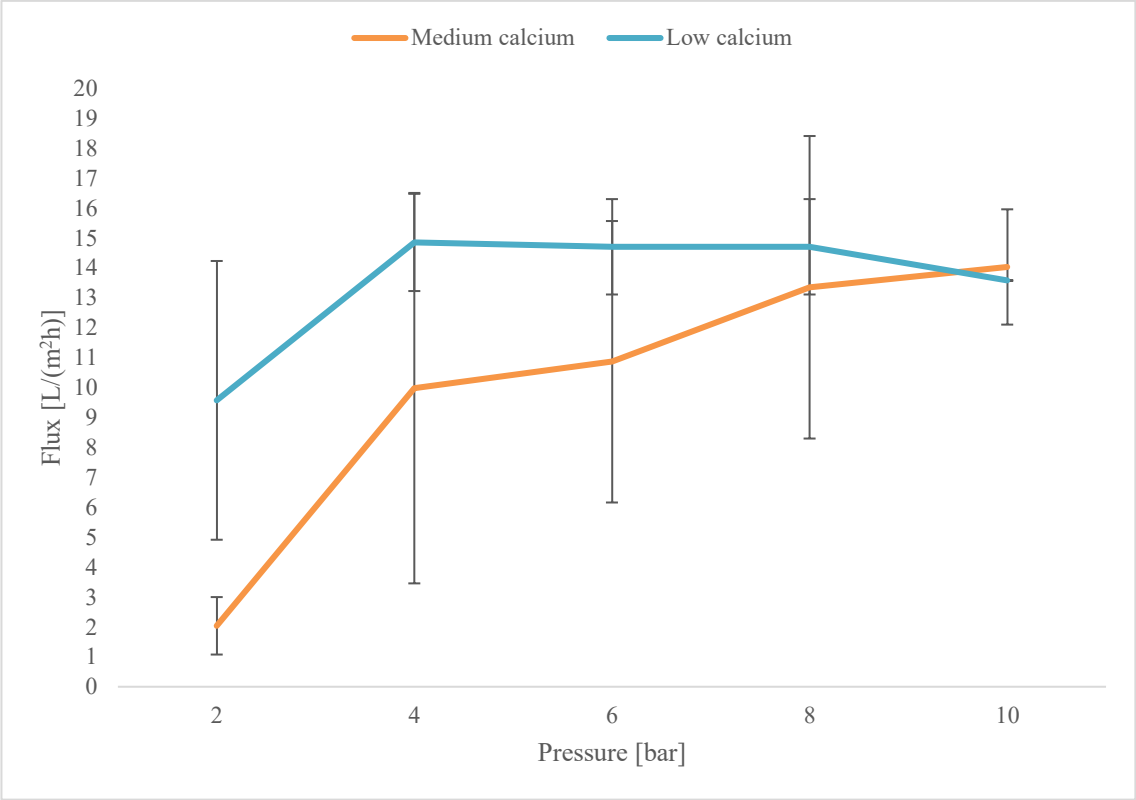

Figure 25. Average fluxes in 200 – 1000 kPa pressure (T=20°C).

In low pressures (200 – 400 kPa), the flux increased rapidly for both membranes. After 400 kPa, the flux of low-calcium membrane remained in ca. 15 L/m^2h^{-1}. The flux through the medium-calcium membrane increased with the pressure throughout the experiment – however, the slope of the curve was not as steep as between 200 – 400 kPa. The medium-calcium membrane flux was lower than low-calcium membrane flux all the way until 1000 kPa. The standard deviation of results is high; however, this may be due to the low permeate volumes (0.1 – 1.26 mL/min), as a single droplet of permeate had a notable effect on the collected sample volume and getting exact readings with a graduated cylinder was challenging.

Next, the pressure of the system was set to be constant (200 kPa) and the previous experiment was repeated in temperature range 20 – 60°C. The obtained average fluxes with standard deviation are presented in Figures 26 & 27.

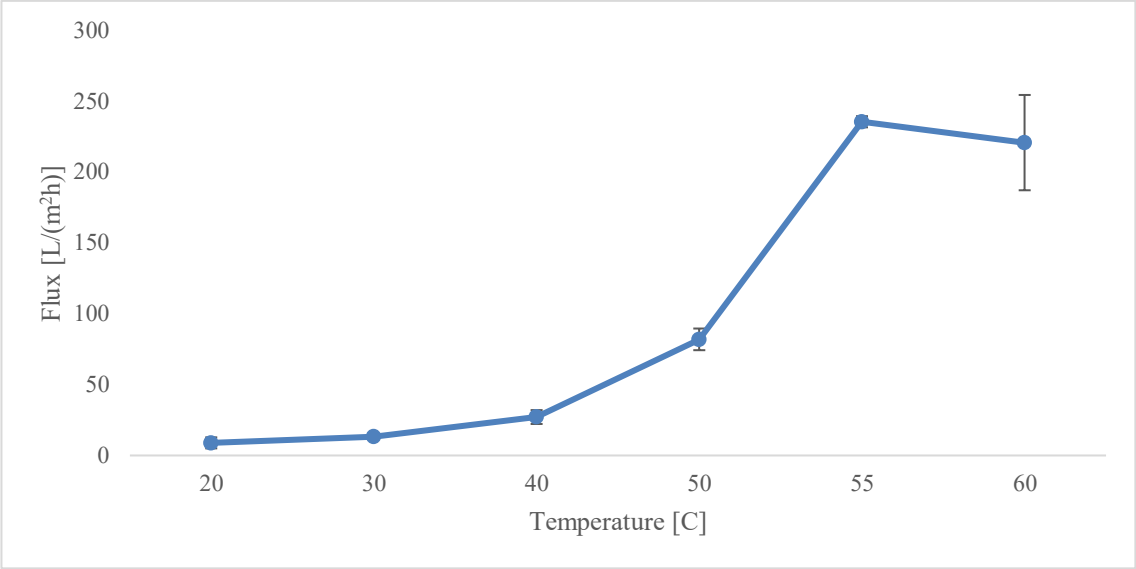

Figure 26. Water flux for low-calcium membrane in 20 – 60°C and constant 200 kPa pressure.

The low-calcium membrane flux showed high dependency on the temperature: The flux increased steadily from 8.9 L/m^2h^{-1} to 27.1 L/m^2h^{-1} in range 20 – 40°C. In temperatures above 50°C fluxes of 200 – 230 L/m^2h^{-1} were measured. The sharp increase in flux is likely caused by breaking of the membranes: After the experiment, the membranes had visible cracks and fractures.

As none of the low-calcium membranes stayed intact in high temperatures, it can be deduced that the thermal durability of the low-calcium membranes was low. Cracking and fracturing are plausible explanations for the relatively high standard deviation (3.9 – 33) in 40 – 60°C temperatures, as the cracks expanded at different rates.

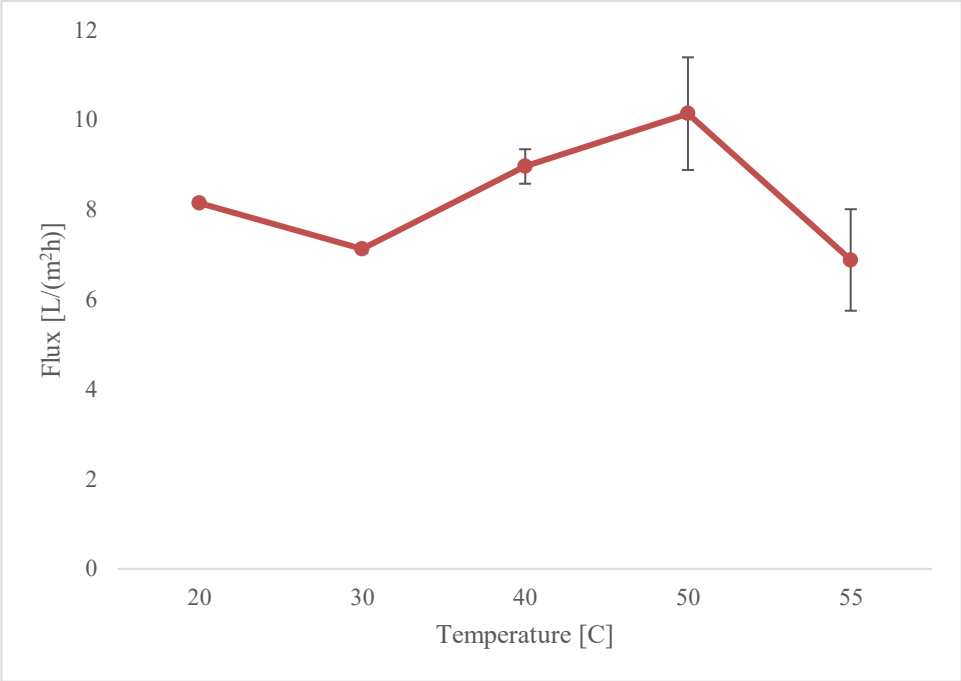

Figure 27. Water flux for medium-calcium membrane in 20 – 60°C and constant 200 kPa pressure.

The flux through the medium-calcium membranes remained low (6 – 10 L/m^2h^{-1}) in the whole temperature range 20 – 60°C. The highest obtained flux for medium-calcium membranes was 10.1 L/m^2h^{-1} in 50°C. The medium-calcium membranes seemed to endure the high temperatures well and none of the membranes broke in the experiments. Standard deviation is moderate (0.09 – 1.25) and the overall trend is consistent.

Despite the water flux results being reasonable, substantial differences in the permeate fluxes were observed in the solution filtration experiments: In some cases, the flux was virtually zero for no obvious reason. Significant differences in flux also existed between membranes from same preparation batch. Accumulation of grinding dust in the pores was one suspected reason for the inconsistencies in flux. However, an ultrasonic bath or blowing pressurized air through the membrane had no perceivable effect on the flux.

Another plausible explanation for the inconsistent flux is variation in the preparation method. As mentioned in 5.1.4, the grinding time and pressure were not standardized, and membranes were cast at different heights. The density of the membranes may vary as some membranes received more grinding either on the permeate or retentate side of the

membrane. Standardized grinding time and pressure and polishing with finer abrasive papers (P600 or higher) could level out differences between individual membranes.

5.2.2 pH neutralization

The goal of the pH neutralization experiment was to determine the permeate volume of 0.1 M acetic acid solution required to neutralize the membrane. The membrane was considered neutralized when the pH of water permeating through the membrane was 7 – 8.5. Initial experiments were conducted by soaking the membrane in turns in acetic acid solution and deionized water to determine roughly which material required longer filtration time. The initial pH of the deionized water the low-calcium-membrane was submerged in was 12.36, and 12.08 for the medium-calcium membrane.

The low-calcium-membrane was neutralized after 34.2 mL of 0.1 M acetic acid had permeated. Total acid filtration time was 50 minutes. The target pH (7.68) was achieved by running through the sequence explained in chapter 4.3.2. three times (20 min + 20 min + 10 min acid filtrations with rinsing in between).

Initial experiments indicated that the medium-calcium-membranes would require more acid and longer treatment to neutralize. Total of 45.8 mL 0.1 M acetic acid and 230 min filtration time was required to neutralize the medium-calcium-membrane. pH 7.81 was achieved by running through the sequence twice.

The chemical resistance of the membranes appeared to be low in the acetic acid filtrations: All membranes that were treated with acid became extremely brittle, and broke either during or right after the treatment, and the treated membranes could not be used in other experiments. As the membranes for solution filtration experiments were not neutralized, it is essential to note that this might affect the membrane performance due to the higher solubility of some substances (e.g., humic acid) to water in high pH. The poor chemical durability of the membranes was an unexpected finding, as geopolymer materials, such as foams, have been successfully neutralized earlier (Szechyńska-Hebda 2019), and the reason behind the poor chemical durability of the membranes remains a mystery. The breaking of the membranes during or right after acid treatment may be due to the combination of room temperature curing, thinness of the membranes and the long period of acid filtration time at slightly elevated pressure.

5.2.3 Humic acid filtration

The results from humic acid filtration experiments are conflicting: According to the UV-VIS measurements and the DOC measurements done in an external laboratory, the organic content of permeate stream was higher than the retentate stream or the feed solution. The membrane itself seemed to contaminate the permeate; When pure, deionized water was filtrated with an un-used membrane, readings of 25-44 mg/L were obtained from permeate with UV-VIS. Clear origin of the organic contamination was not found, but suspected reasons for the high organic content are membrane contamination from mould oil or the laboratory grease used in the O-ring seals of the filtration unit.

The results from humic acid filtrations are presented in Figures 28 – 31. The retentate concentrations remained on a steady level very close to the feed concentration in the UV-VIS experiments (20-25 mg/L) and the permeate concentrations increased from 20 mg/L to 28 mg/L for low-calcium membrane and from 30 mg/ L to 39 mg/L for medium-calcium membrane.

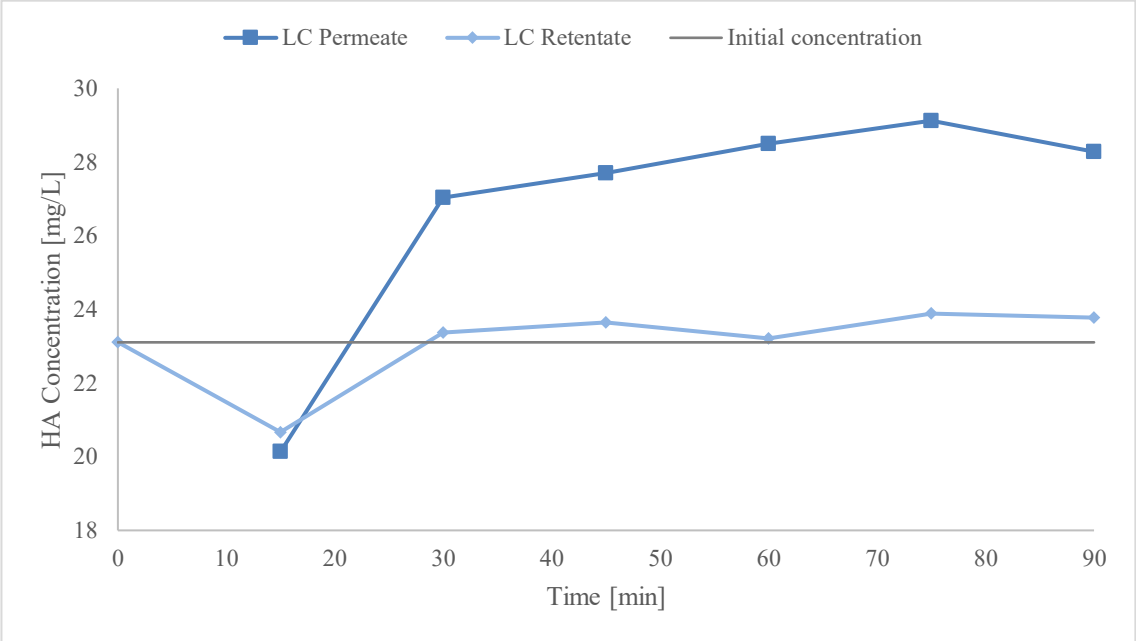

Figure 28. Humic acid concentration (UV-VIS), low-calcium-membrane.

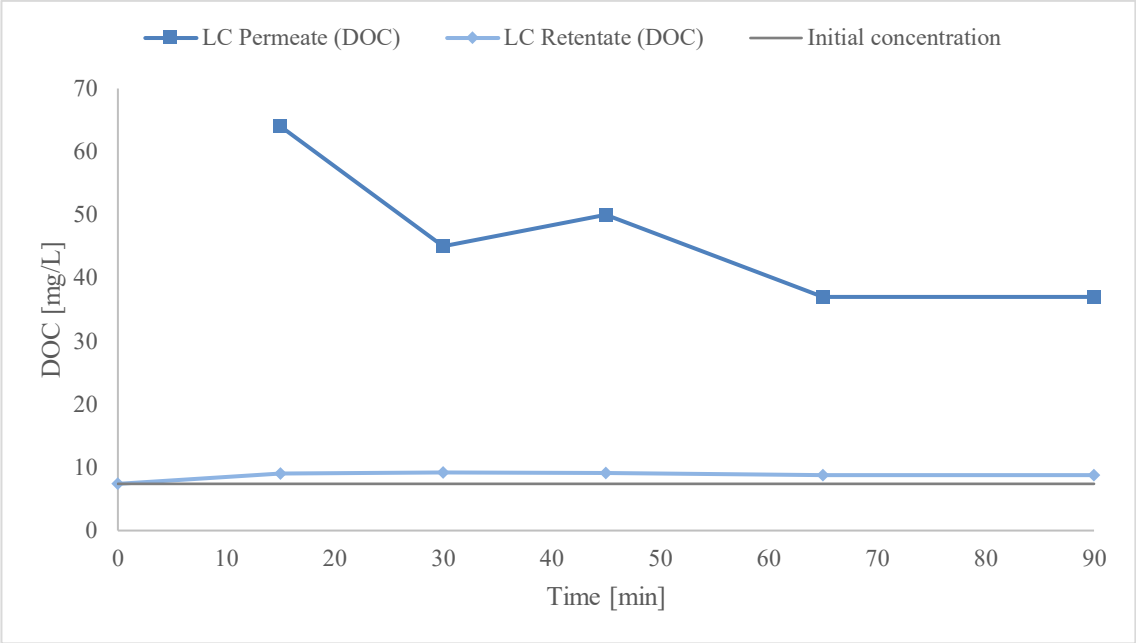

Figure 29. Dissolved organic carbon in humic acid filtration with low-calcium membrane.

In the external DOC measurements, the retentate concentration was only around 5 – 10 mg/L and the permeate concentration varied between 30 – 65 mg/L. The contamination seemed to be the worst in the low-calcium DOC experiment, as the permeate concentration was 64 mg/L at the beginning and gradually dropped to 37 mg/L as the experiment proceeded.

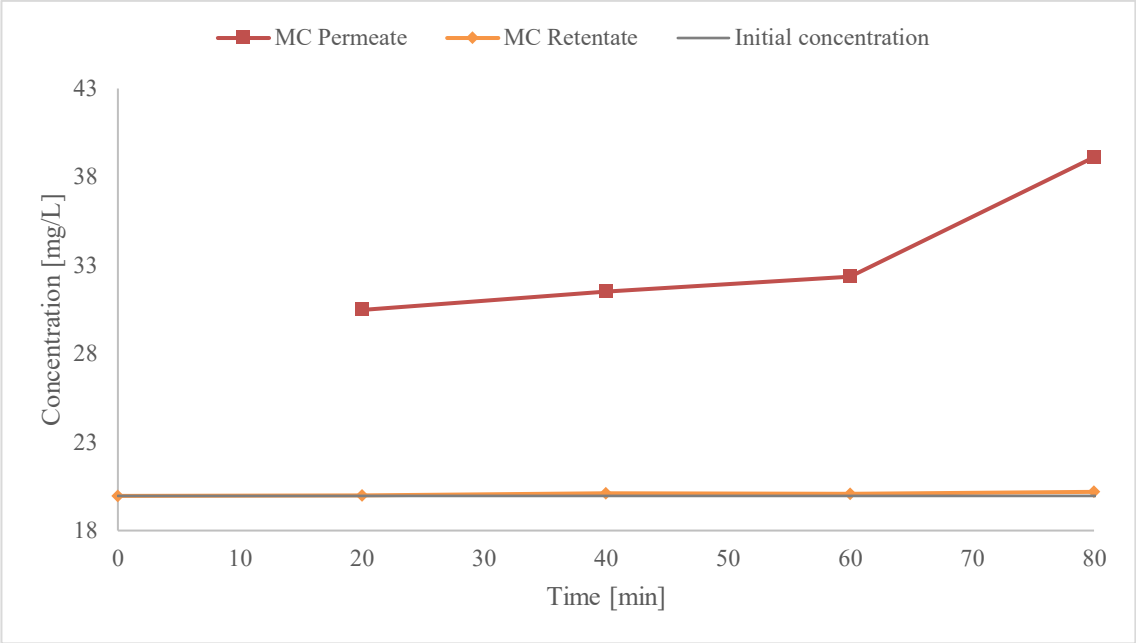

Figure 30. Humic acid concentration (UV-VIS), medium-calcium-membrane.

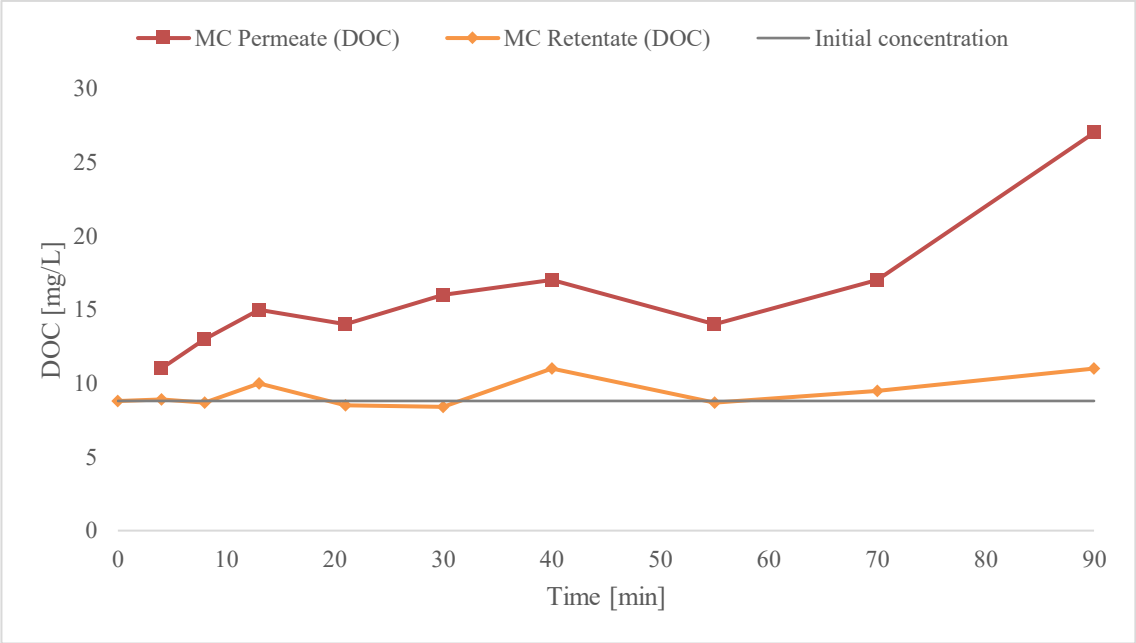

Figure 31. Dissolved organic carbon in humic acid filtration with medium-calcium membrane.

There was an increase in the permeate concentration towards the end of the experiment in all except one of the experiments (highly contaminated low-calcium DOC test), which indicates that despite the contamination, the membrane did in fact retain some humic acid at the beginning of the experiment. As the membrane fouled, humic acid began permeating through the membrane.

The flux declined for both membranes, (Figure 32) which is a strong indicator of membrane fouling. The relative decrease in flux was very similar for both membranes; the flux declined 83 % for low-calcium membrane, whereas for medium-calcium membrane the decline was 80 %. The curve of decline was steeper for the low-calcium membrane during the first 10 minutes, as the initial flux was higher.

However, as the contamination compromises the results, no definite conclusions on fouling or the separation performance can be drawn from the results.

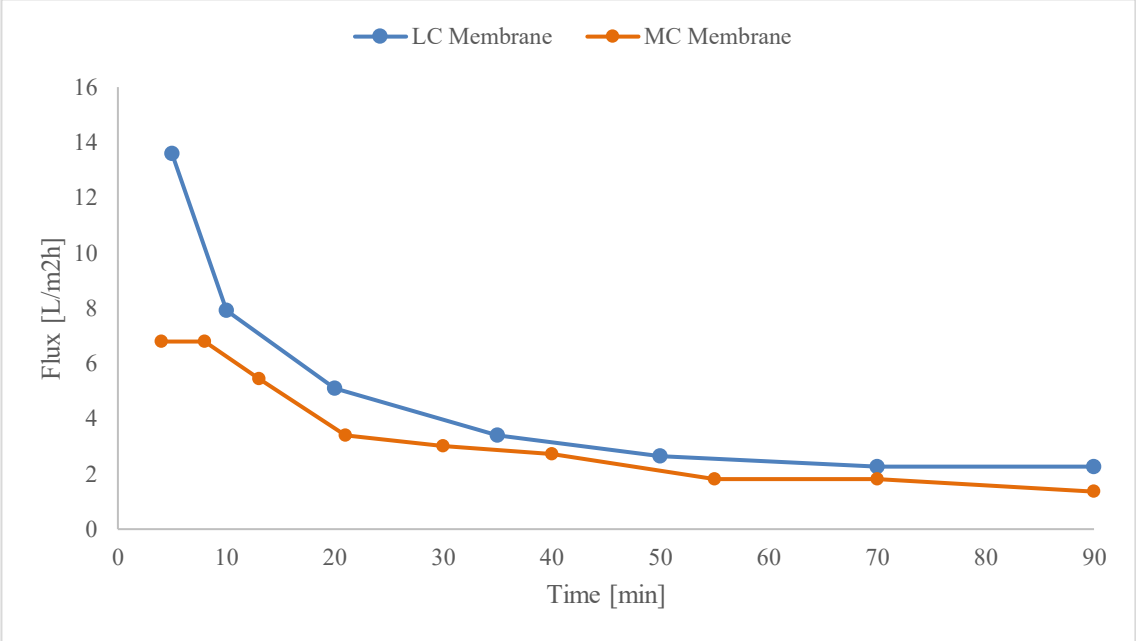

Figure 32. Development of flux in humic acid filtrations.

5.2.4 Ammonium ion solution filtration

The goal of ammonium ion solution filtration experiment was to see if the membranes are suitable for removal of ammonium ions from water. All samples were diluted with 1:25

ratio to obtain the 25 mL volume required for the analysis. 50 mg/L ammonium ion solution was prepared and used as a feed fluid, and the initial concentration of the retentate was measured for at t=0 min and this value was used as the actual initial concentration to ensure the same level of error in all measurements. Some error exists in the results, as the accuracy of the analyser varied by few units when measuring the concentration of standard solutions (10 mg/L and 100 mg/L) and it is reasonable to expect that the error may accumulate when using dilutions. The measured initial concentration is marked in the result figures.

Both membranes were able to retain ammonium ions to some extent, even though the membrane performance decreased rapidly. For low-calcium membrane, the maximum separation performance was achieved during the first three minutes of filtration, as the ammonium ion concentration in retentate rose to 98.73 mg/L from the initial retentate concentration 80.80 mg/L. At three-minute mark, the permeate concentration was 12.76 mg/L. After the first few minutes, the retentate concentration began decreasing, finally achieving 53.37 mg/L after 90 minutes of filtration, while permeate concentration increased up to 41.63 mg/L. The results for low-calcium membrane are shown in Figure 33.

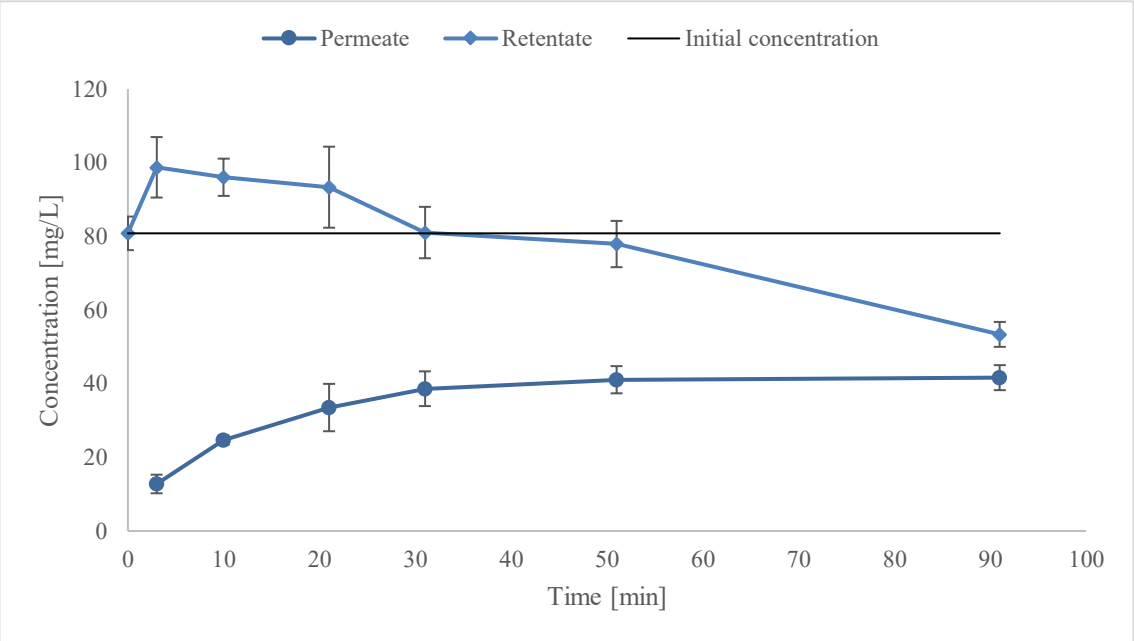

Figure 33. Ammonium ion concentration, low-calcium-membrane with standard deviation.

Medium-calcium membrane behaved very similarly during the first few minutes (Figure 34). The maximum separation performance was achieved after first four minutes: Retentate concentration increased from 87.35 mg/L to 108.38 mg/L, while permeate concentration was low, 14.18 mg/L. The membrane performance declined rapidly: After 55 minutes of filtration, the retentate concentration had decreased to 83.80 mg/L while permeate concentration increased to 75.60 mg/L. At the end of the experiment at 90 minutes, the concentrations were almost the same: Permeate being 64.40 mg/L and retentate 64.80 mg/L.

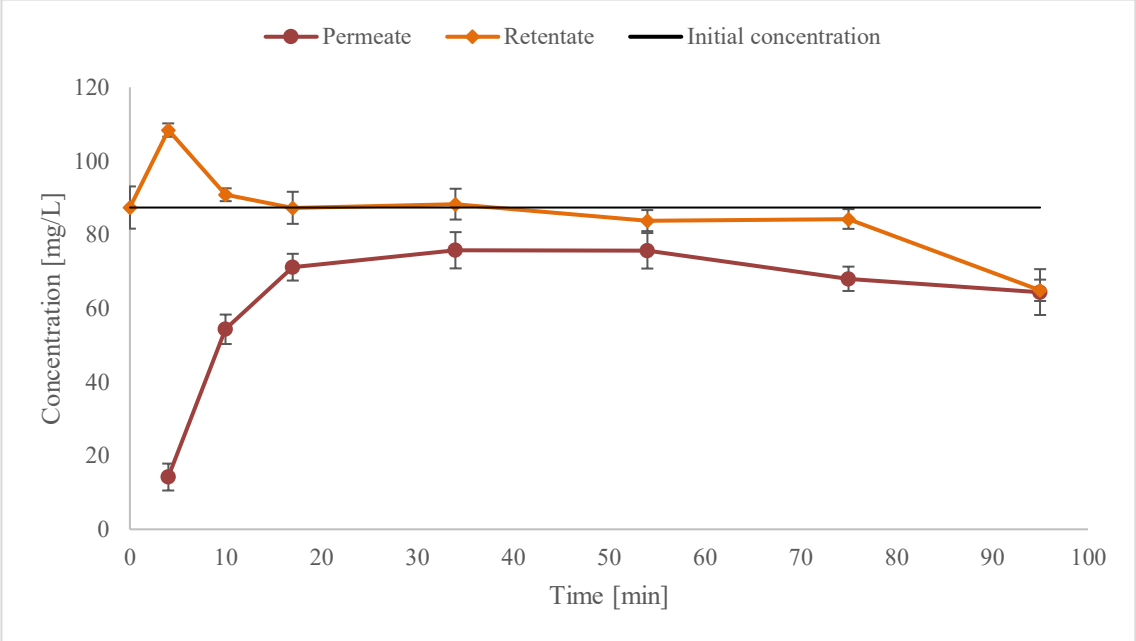

Figure 34. Ammonium ion concentration, medium-calcium-membrane with standard deviation.

Considering the mass balance of the batch-wise operated filtration system, the total mass of ammonium in the feed solution, m_{feed}, is based on the measured initial concentrations and the 500 mL feed volume. If the collected sample volume is estimated to be 2 mL per sample for permeate and 4 mL per sample for retentate, the mass of ammonium that was extracted from the system through permeate, $m_{p,\,out}$, and mass of ammonium that was extracted from the system through retentate, $m_{r,\,out}$, can be calculated from the measured concentrations. During the experiment, the part of retentate which was not removed from

the tank as samples, was continuously circulated back to the filtration unit. The volume of solution remaining in the filtration unit at the end of the experiment can be calculated by reducing the collected sample volumes from feed volume, and the amount of ammonium remaining in the tank, m_{tank}, can be calculated based on the final retentate concentration.

Roughly estimated mass balance for the filtration system is shown in Table 6 and an illustration of the system is shown in Figure 35.

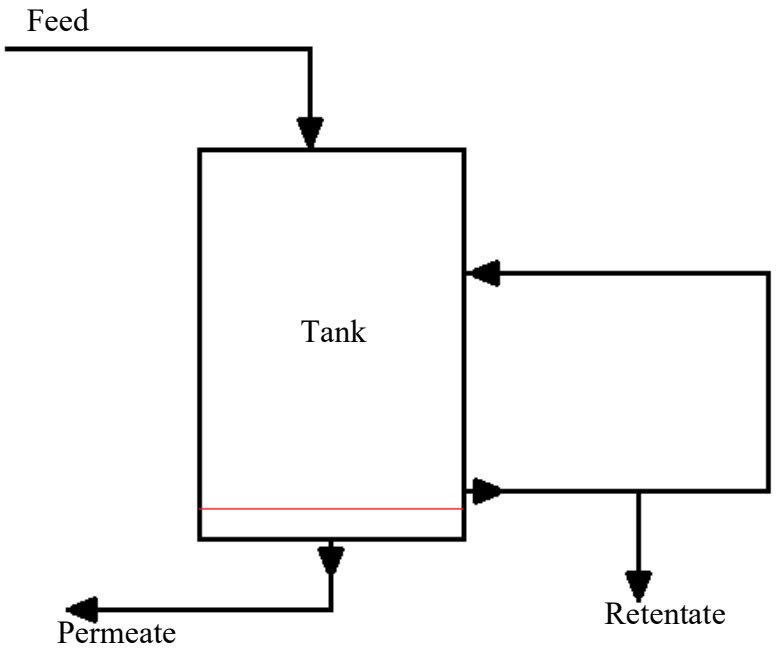

Figure 35. Illustration of the filtration system.

According to conservation of mass, the mass leaving the system, m_{out} and m_{tank}, should be equal to the mass entering the system, m_{feed}. The difference between mass entering and mass leaving suggests that some ammonium ions were adsorbed inside the membrane – however, as the calculations are based on estimates, some error still exists, and it cannot be determined exactly how much of the mass was adsorbed.

Table 6. Estimate on the mass balance of the filtration system [mg].

	Low-calcium membrane	**Medium-calcium membrane**
m_{feed}	40.4	43.68
$m_{p,\ out}$	0.38	0.85
$mr_{,\ out}$	1.00	1.39
m_{tank}	24.76	29.72
Adsorbed amount	14.26	11.72

Membrane fouling occurred soon after the beginning of the experiment. The flux of low-calcium membrane decreased 40 % during first 30 minutes and then remained around 5 L/m^2h^{-1} for the rest of the experiment. For medium-calcium membrane the decline was steeper: The membrane lost 43 % of flux during first ten minutes. The final flux for medium-calcium membrane was 2.04 L/m^2h^{-1}. For both membranes, the flux and the ammonium ion concentration levelled at the same time – for low-calcium membrane, the flux and ammonium ion concentrations remained steady after 30 minutes of filtration, and after 20 minutes for medium-calcium membrane. The development of flux in shown in Figure 36.

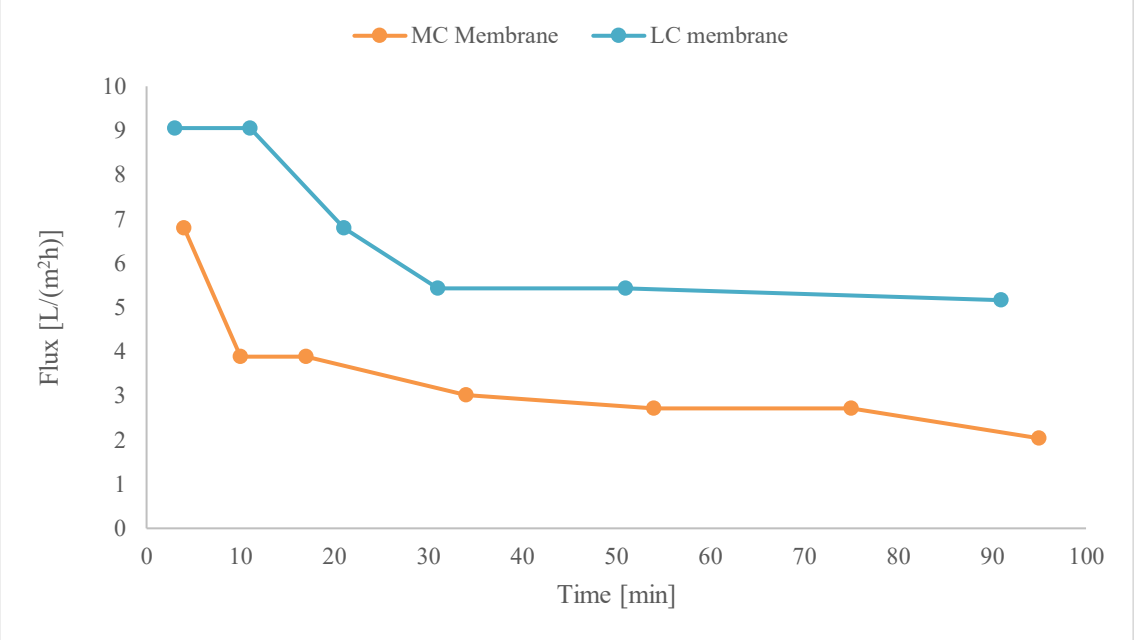

Figure 36. Development of flux in ammonium filtration experiments.

The level of contamination was evaluated by filtrating deionized water and measuring the ammonium ion concentration. The measured ammonium ion concentration was practically zero for both membranes, so in this case, the results are reliable and comparable. Both membranes retained ammonium ions and the maximum separation performance was achieved within first few minutes of the experiments. After approximately 20 minutes, the permeate concentrations, and fluxes, for both membranes stabilized and remained consistent until the end of the experiment.

6 CONCLUSIONS

The purpose of this thesis was to investigate the suitability of alkali-activated materials as membrane materials. Initial experiments were performed for three materials: Low-calcium material based on metakaolin, medium-calcium material based on metakaolin, and blast furnace slag and high-calcium material based on blast furnace slag. High-calcium material showed tendency to crack and break easily and it was left out from rest of the experiments. The structure, mineralogy and mechanical properties of low-calcium and medium-calcium materials was explored with accustomed characterization methods, and the separation performance of the materials was tested with a series of filtration experiments.

The microstructural and mineralogical characterization of the membrane materials was based on XRD, and SEM. Porosity of the materials was investigated with BET and BHJ, and the membrane charge was studied via a zeta-potential measurements. The mechanical properties were examined in flexural and compressive strength tests, and by measuring the shrinkage and change in mass during a 30-day period.

In the second stage of the thesis, the separation performance of the prepared membranes was studied. First, the permeation of deionized water through the membranes was investigated in different temperature and pressure conditions. Next, attempts were made to neutralize the membranes by filtrating mild acetic acid, as alkali-activated materials are highly alkaline by nature, which may hamper the separation, as the solubility of substances in aqueous solutions depends on the pH. Finally, humic acid and ammonium ion solution were filtrated to determine if the membranes were capable to retain organic or ionic substances from water.

The main finding of the thesis was that both membrane materials did retain ammonium ions to some extent, and the separation was achieved without any optimization, such as purification or neutralization, of the membranes. The separation performance can undoubtedly be further improved by optimizing the membranes. The contamination of the humic acid samples weakened the reliability of the humic acid filtration results – however, the decline in flux and constantly increasing permeate concentration suggest that membrane fouling occurred, and the fouling of the membranes is an indicator of

retaining humic acid. However, reliable and clear conclusions cannot be drawn from the results due to contamination.

Generally, the low-calcium membrane showed better performance for membrane filtration applications. The fluxes through low-calcium membrane were higher than through medium-calcium membrane, and the rate of fouling – indicated by decline in flux and increase of concentration in permeate – was slightly lower than for medium-calcium membrane.

In terms of mechanical and thermal durability, the medium-calcium showed better performance. Low-calcium membraned cracked in high temperature filtrations and broke easily in demoulding. Higher mechanical durability could be achieved by increasing the curing temperature, as suggested by earlier literature. Chemical resistance of the membranes was tested in neutralization experiments, and neither of the membranes endured treatment with mild acid. The stability of the medium-calcium membrane was slightly lower than that of the low-calcium membrane, as the presence of calcium carbonate crystals may hinder the separation performance in certain process conditions.

Overall, the results of this thesis suggest that alkali-activated materials are a promising and suitable alternative as a membrane filtration material. The fabrication process of alkali-activated membranes is extremely simple, and membranes with satisfactory mechanical, chemical, and thermal durability can be obtained with room-temperature curing. The main challenge in this thesis was the cracking of the membranes as they dried in storage, and the membranes had to be preserved in high moisture and wrapped in plastic. However, storing geopolymer membranes submerged in water or in high humidity is not an issue in most industrial membrane applications, as the membranes can be easily sealed in plastic.

A variety of challenges was faced in the practical phase of the thesis. The brittleness caused by drying was a major challenge, and the curing temperature had to be set to room temperature to ensure that all samples endured curing without cracking. However, low curing temperature compromises the mechanical properties of the material, which later caused issues in demoulding and grinding. The demoulding process itself was quite complicated, as the shape of the moulds made it difficult to demould the membranes. Getting the samples out of the moulds required force and pressurized air, and several

samples broke in demoulding, or later in grinding. Changing the mould type from petri dish to a 3D-printed “cake tin” could eliminate, or at least minimize, the breaking of membranes in demoulding. Dismountable mould would also enable lower casting height of the membranes, and less grinding would be needed to fit the membranes in the filtration unit, again eliminating one breaking-sensitive step from the preparation process. Also, as mould oil was the suspected origin of the organic contamination observed in UV-VIS measurements, applying a different type of mould that does not require oil could yield more reliable results.

Despite the many challenges faced in the process, alkali-activated low-calcium and medium-calcium materials appear to be effective in membrane filtration. The synthesis of the membranes is very economical compared to conventional ceramic membranes, as the raw materials metakaolin and blast furnace slag are abundant and relatively inexpensive, and the energy consumption of the room-temperature preparation process is low. Considering practical applications, the main challenges were the poor chemical resistance of the membranes, and the tendency of the thin membranes to crack when exposed to air and drying.

REFERENCES

Azarshab, M., Mohammadi, F., Maghsoodloorad, H. & Mohammadi, T. 2016. Ceramic membrane synthesis based on alkali-activated blast furnace slag for separation of water from ethanol. Ceramics International, 42(14), pp. 15568-15574.

Bai, C. & Colombo, P. 2017. High-porosity geopolymer membrane supports by peroxide route with the addition of egg white as surfactant. Ceramics International, 43(2), pp. 2267-2273.

Baker, R.W., 2012. Membrane Technology and Applications. 3rd ed. United Kingdom: John Wiley and Sons Ltd, 575 p. 575.

Bakria, A. M. A., Kamarudin, H., BinHussain, M., Nizar, I., Zarina, Y. & Rafiza, A. 2011. The effect of curing temperature on physical and chemical properties of geopolymers. Physics Procedia, 22, pp. 286-291.

Barredo-Damas, S., Alcaina-Miranda, M. I., Gemma, M., Iborra-Clar, M. I. & Mendoza-Roca, J. A. 2011. Influence of operating conditions on ceramic ultrafiltration membrane performance when treating textile effluents. Water Science And Technology, 64(11), pp. 2169-2176.

Bella, N., Gudiel, E., Soriano, L., Font, A., Borrachero, M. V., Paya, J. & Monzó, J. M. 2020. Formulation of alkali-activated slag binder destined for use in developing countries. Applied Sciences, 10, p. 9088.

Benavent, V., Frizon, F. & Poulesquen, A. 2016. Effect of composition and aging on the porous structure of metakaolin-based geopolymers. Journal Of Applied Crystallography, 49(6), pp. 2116-2128.

Bernal, S. A. & Provis, J. L. 2014. Durability of alkali-activated materials: progress and perspectives. Journal Of The American Ceramic Society, 97(4), pp. 997-1008.

Chaouche, M., Gao, X. X., Cyr, M., Cotte, M. & Frouin, L. 2017. On the origin of the blue/green color of blast-furnace slag-based materials: Sulfur K-edge XANES investigation. Journal Of The American Ceramic Society, 100(4), pp. 1707-1716.

Chen, L., Wang, Z., Wang, Y. & Feng, J. 2016. Preparation and properties of alkali activated metakaolin-based geopolymer. Materials, 9(9), p. 767.

Cheryan, M. 1986. Ultrafiltration Handbook. Lancaster, Pa.: Technomic Publishing Co.

Cho, B., Koo, K. & Choi, S. 2018. Compressive strength and microstructure properties of alkali-activated systems with blast furnace slag, desulfurization slag, and gypsum. Advances In Civil Engineering, 2018, pp. 1-9.

Coto, B., Martos, C., Peña, J., Rodríguez, R. & Pastor, G. 2012. Effects in the solubility of CaCO3: Experimental study and model description. Fluid Phase Equilibria, 324, pp. 1-7.

Cullity, B. D. & Stock, S. R. 2001. Elements Of X-Ray Diffraction. 3rd ed. Upper Saddle River (NJ): Prentice Hall.

Davidovits, J., 1991. Geopolymers: Inorganic polymeric new materials. Journal Of Thermal Analysis, 37, pp. 1633-1656.

Davidovits, J. 2015. Geopolymer chemistry and applications. 4th edition. Saint-Quentin: Institut Géopolymère.

Daud, N. A. A., Shamsuddin, M. R. & Pradanawati, S. A. 2021. Synthesis and characterization of fly ash-based geopolymer membrane for methylene blue dye removal. IOP conference series. Earth And Environmental Science, 765(1), p. 12081.

De Andrade, C. J.; Mano, M. C. R.; Paulino, B. N., Pinto, L. L. L., Roslan, J., & Pa'ee. K. F., 2017. An overview on ultrafiltration in food processing. In: Ramirez, J., eds. 2017. Ultrafiltration: Methods, Applications and Insights. New York, US: Nova Science Publishers, Inc, p. 53-111. ISBN: 978-1-53610-624-4

Deer, W. A., Howie, R. A. & Zussman, J. 2013. An Introduction To The Rock-Forming Minerals. 3. ed. London: Mineralogical Society.

Della Rocca, D. G., Peralta, R. M., Peralta, R. A., Rodríguez-Castellón, E. & de Fatima Peralta Muniz Moreira, R. 2020. Adding value to aluminosilicate solid wastes to produce adsorbents, catalysts and filtration membranes for water and wastewater treatment. Journal Of Materials Science, 56(2), pp. 1039-1063.

Domany, Z., Galambos, I., Vatai, G. & Bekassy-Molnar, E. 2002. Humic substances removal from drinking water by membrane filtration. Desalination, 145(1), pp. 333-337.

Duxson, P., Lukey, G. C. & van Deventer, J. S. J. 2007. Physical evolution of Na-geopolymer derived from metakaolin up to 1000 °C. Journal Of Materials Science, 42(9), pp. 3044-3054.

Finland's Environmental Administration, 2019. Teollisuuden päästöt vesistöön vuonna 2017. Available from: https://www.ymparisto.fi/fi-FI/Kartat_ja_tilastot/Vesistojen_kuormitus_ja_luonnon_huuhtouma/Teollisuuden_vesistokuormitus/Teollisuuden_paastot_vesistoon_vuonna_20(50076) [cited 14.6.2021]

Finnsementti Oy, 2019. Masuunikuonajauhe KJ400. Available from: https://finnsementti.fi/wp-content/uploads/2019/02/Masuunikuonajauhe_KJ400.pdf [cited 14.6.2021]

Gao, W., Liang, H., Ma, J., Han, M., Chen, Z., Han, Z. & Li, G. 2011. Membrane fouling control in ultrafiltration technology for drinking water production: A review. Desalination, 272(1), pp. 1-8.

Garcia-Lodeiro, I., Palomo, A. & Fernández-Jiménez, A., 2015. An overview of the chemistry of alkali-activated cement-based binders. In: Pacheco-Torgal, F., Labrincha, J. A., Leonelli, C., Palomo, A. & Chindaprasirt, P., eds. 2015. Handbook Of Alkali-Activated Cements, Mortars And Concretes. Waltham, MA: Woodhead, 19-47. ISBN 978-1-78242-288-4

Ge, Y., Yuan, Y., Wang, K., He, Y. & Cui, X. 2015. Preparation of geopolymer-based inorganic membrane for removing Ni2+ from wastewater. Journal Of Hazardous Materials, 299, pp. 711-718.

Ghosh, K. & Ghosh, P. 2018. Effect of alkali concentration on mechanical properties, microstructure, zeta potential and electrical conductivity of thermally cured fly ash -blast furnace slag based blended geopolymer composites. Oriental Journal Of Chemistry, 34(2), pp. 704-715.

Goren, U., Aharoni, A., Kummel, M., Messalem, R., Mukmenev, I., Brenner, A. & Gitis, V. 2008. Role of membrane pore size in tertiary flocculation/adsorption/ultrafiltration treatment of municipal wastewater. Separation And Purification Technology, 61(2), pp. 193-203.

Gunasekara, C., Law, D. W., Setunge, S. & Sanjayan, J. G. 2015. Zeta potential, gel formation and compressive strength of low calcium fly ash geopolymers. Construction & Building Materials, 95, pp. 592-599.

He, Y., Cui, X., Liu, X., Wang, Y., Zhang, J. & Liu, K. 2013. Preparation of self-supporting NaA zeolite membranes using geopolymers. Journal Of Membrane Science, 447, pp. 66-72.

He, P. Y., Zhang, Y. J., Chen, H., Han, Z. C. & Liu, L. C. 2020. Low-cost and facile synthesis of geopolymer-zeolite composite membrane for chromium(VI) separation from aqueous solution. Journal Of Hazardous Materials, 392, p. 122359.

Hillel, D., Rosenzweig, C., Powlson, D., Scow, K., Singer, M. & Sparks, D., 2004. Encyclopedia Of Soils In The Environment. 1st edition. New York, NY: Academic Press. ISBN 978-0123485304.

Hojati, M., Rajabipour, F. & Radlińska, A. 2019. Drying shrinkage of alkali-activated cements: Effect of humidity and curing temperature. Materials and structures, 52(6).

Ivanovic, M., Kljajevic, L., Gulicovski, J., Petkovic, M., Jankovic-Castvan, I., Bucevac, D. & Nenadovic, S. 2020. The effect of the concentration of alkaline activator and aging

time on the structure of metakaolin based geopolymer. Science Of Sintering, 52(2), pp. 219-229.

Jeantelot, G., Ould-Chikh, S., Sofack-Kreutzer, J., Abou-Hamad, E., Anjum, D. H., Lopatin, S., . . . Basset, J. 2018. Morphology control of anatase TiO2 for well-defined surface chemistry. Physical Chemistry Chemical Physics: PCCP, 20(21), pp. 14362-14373.

Jia, D., He, P., Wang, M. & Yan, S., 2020. Geopolymer and Geopolymer Matrix Composites. Singapore: Springer. ISBN 978-981-15-9536-3.

Kara, I., Tunc, D., Sayin, F. & Akar, S. T. 2018. Study on the performance of metakaolin based geopolymer for Mn(II) and Co(II) removal. Applied Clay Science, 161, pp. 184-193.

Kim, B. & Lee, S. 2020. Review on characteristics of metakaolin-based geopolymer and fast setting. Han'guk Seramik Hakhoe chi, 57(4), pp. 368-377.

Kumar, R. & Ismail, A. F. 2015. Fouling control on microfiltration/ultrafiltration membranes: Effects of morphology, hydrophilicity, and charge. Journal Of Applied Polymer Science, 132(21), pp. -n/a.

Lee, M., Wu, Z., Li, K., 2015. Advances in ceramic membranes for water treatment. In: Basile, A., Cassano, A., Rastogi, N.K., eds. 2015. Advances In Membrane Technologies For Water Treatment: Materials, Processes And Applications. United Kingdom: Elsevier Ltd, 43-82. ISBN 978-1-78242-126-9.

Lin, J. & Zhan, Y. 2012. Adsorption of humic acid from aqueous solution onto unmodified and surfactant-modified chitosan/zeolite composites. Chemical Engineering Journal (Lausanne, Switzerland : 1996), 200-202, pp. 202-213.

Luukkonen, T., Heponiemi, A., Runtti, H., Pesonen, J., Yliniemi, J. & Lassi, U. 2019. Application of alkali-activated materials for water and wastewater treatment: A review. Reviews In Environmental Science And Biotechnology, 18(2), pp. 271-297.

Madaeni, S.S., Ghaemi, N., Rajabi, H., 2015. Advances in polymeric membranes for water treatment. In: Basile, A., Cassano, A., Rastogi, N.K., eds. 2015. Advances In Membrane Technologies For Water Treatment: Materials, Processes And Applications. United Kingdom: Elsevier Ltd, 3-41. ISBN 978-1-78242-126-9.

Mastali, M., Kinnunen, P., Dalvand, A., Mohammadi Firouz, R. & Illikainen, M. 2018. Drying shrinkage in alkali-activated binders – A critical review. Construction & Building Materials, 190, pp. 533-550.

Metcalf & Eddy, Tchobanoglous, G., Stensel, H. D., Tsuchihashi, R., Burton, F. L., Abu-Orf, M., Bowden, G. & Pfrang, W. 2014. Wastewater Engineering: Treatment And Resource Recovery. 5. ed. New York, NY: McGraw-Hill Education.

Moulik, S., Parakala, S. & Sridhar, S., 2019. Tackling challenging industrial separation problems through membrane technology. In: Sridhar, S. & Moulik, S.(toim.) Membrane Processes: Pervaporation, Vapor Permeation and Membrane Distillation for Industrial Scale Separations. Hoboken, New Jersey, Yhdysvallat: Scrivener Publishing LLC. pp. 1-36. ISBN 978-1-119-41822-1.

Nascimento, T. A., Mejía, F. R., Fdz-Polanco, F. & Peña Miranda, M. 2017. Improvement of municipal wastewater pretreatment by direct membrane filtration. Environmental Technology, 38(20), pp. 2562-2572.

Pal, S., Mukherjee, A. & Pathak, S. 2003. Investigation of hydraulic activity of ground granulated blast furnace slag in concrete. Cement And Concrete Research, 33(9), pp. 1481-1486.

Pimraksa, K., Setthaya, N., Thala, M., Chindaprasirt, P. & Murayama, M. 2020. Geopolymer/Zeolite composite materials with adsorptive and photocatalytic properties for dye removal.(Research Article). Plos One, 15(10), p. e0241603.

Provis, J.L., 2014. Introduction and scope. In: Provis, J. & Deventer, J. S. v. 2014. Alkali Activated Materials: State-Of-The-Art Report, RILEM TC 224-AAM. New York: Springer, 1-9. ISBN 978-94-007-7672-2.

Provis, J.L., Yong, S.L. & Duxson, P., 2009. Nanostructure/microstructure of metakaolin geopolymers. In: Provis, J.l. & van Deventer, J.S.J, 2009. Geopolymers: Structure, Processing, Properties And Industrial Applications. Cambridge, Uk: Woodhead Publishing, 72-88. ISBN 978-1-84569-638-2.

Provis, J.L., Duxson, P., Kavalerova, E., Krivenko, P.V., Pan, Z., Puertas, F., & van Deventer, J.S.J., 2014. Historical aspects and overview. In: Provis, J. & Deventer, J. S. v. 2014. Alkali Activated Materials: State-Of-The-Art Report, RILEM TC 224-AAM. New York: Springer, 11-59. ISBN 978-94-007-7672-2.

Purkait, M.K. & Singh, R., 2018. Membrane Technology in Separation Science. 1st ed. Boca Raton, US: Taylor & Francis Group, LLC, 2018. ISBN 978-1-138-62626-3.

Rashad, A. M. 2013. Metakaolin as cementitious material: History, scours, production and composition – A comprehensive overview. Construction & Building Materials, 41, pp. 303-318.

Reed, S. J. B. 1996. Electron Microprobe Analysis And Scanning Electron Microscopy In Geology. Cambridge: Cambridge University Press.

Sablani, S., Goosen, M., Al-Belushi, R. & Wilf, M. 2001. Concentration polarization in ultrafiltration and reverse osmosis: A critical review. Desalination, 141(3), pp. 269-289.

Scott, K., 1996. Overview of the application of synthetic membrane processes. In: Scott, K. & Hughes, R. (toim.) Industrial Membrane Separation Technology. 1. painos. Dordrecht, Hollanti: Springer Science+Business Media. S. 8-31. ISBN 978-94-010-4274-1.

Seader, J.D., Henley, E.J. & Roper, D.K., 2011. Separation Process Principles. 3. painos. Hoboken, New Jersey, Yhdysvallat: John Wiley & Sons Inc. 821 s. ISBN 978-0-470-48183-7.

Shao, N., Tang, S., Li, S., Chen, H. & Zhang, Z. 2020. Defective analcime/geopolymer composite membrane derived from fly ash for ultrafast and highly efficient filtration of organic pollutants. Journal Of Hazardous Materials, 388, p. 121736.

Shi, C., Roy, D. & Krivenko, P., 2006. Alkali-Activated Cements and Concretes. Hoboken: Taylor and Francis. ISBN 978-04-291-8071-2.

Singh, R. 2015. Membrane Technology And Engineering For Water Purification: Application, Systems Design And Operation. 2nd ed. Kidlington, England; Waltham, Massachusetts: Butterworth-Heinemann.

Speth, T.F. & Reiss, C.R., 2005. Water quality. In: American Water Works Association, eds. ,2005. Microfiltration and ultrafiltration membranes for drinking water. Denver, CO: American Water Works Association.

Subaer, Haris, A., Irhamsyah, A., Permatasari, A. D., Desa, S. S., Irfanita, R. & Wahyuni, S. 2020. Pervaporation membrane based on laterite zeolite-geopolymer for ethanol-water separation. Journal Of Cleaner Production, 249, p. 119413.

Sutzkover-Gutman, I., Hasson, D. & Semiat, R. 2010. Humic substances fouling in ultrafiltration processes. Desalination, 261(3), pp. 218-231.

Szechyńska-Hebda, M., Marczyk, J., Ziejewska, C., Hordyńska, N., Mikuła, J. & Hebda, M. 2019. Optimal design of pH-neutral geopolymer foams for their use in ecological plant cultivation systems. Materials, 12(18), p. 2999.

Van Deventer, J., Provis, J., Duxson, P. & Lukey, G. 2007. Reaction mechanisms in the geopolymeric conversion of inorganic waste to useful products. Journal Of Hazardous Materials, 139(3), pp. 506-513.

Whitting, James, 1895. Manufacture of Cement. United States Patent, US544706A.

Williams, P.M., 2016. Membrane charge (zeta potential) effect. In: Drioli, E. & Giorno, L. (eds.) Encyclopedia of Membranes. 1st ed. Heidelberg, Berlin: Springer. P. 1185-1186. ISBN 978-3-662-44325-5.

Xu, M., He, Y., Wang, C., He, X., He, X., Liu, J. & Cui, X. 2015. Preparation and characterization of a self-supporting inorganic membrane based on metakaolin-based geopolymers. Applied Clay Science, 115, pp. 254-259.

Xu, M., He, Y., Liu, Z., Tong, Z. & Cui, X. 2019. Preparation of geopolymer inorganic membrane and purification of pulp-papermaking green liquor. Applied Clay Science, 168, pp. 269-275.

Yan, H., Xue-min, C., jin, M., Liu, L., Liu, X. & Chen, J. 2012. The hydrothermal transformation of solid geopolymers into zeolites. Microporous And Mesoporous Materials, 161, pp. 187-192.

Yang, S. & Du, X. 2019. Enhanced dispersion of carbon nanotubes in water by plasma induced graft poly(N,N-dimethylacrylamide) and its application in humic acid capture. Journal Of Molecular Liquids, 277, pp. 380-387.

Zhang, J., Giorno, L. & Drioli, E. 2006. Study of a hybrid process combining PACs and membrane operations for antibiotic wastewater treatment. Desalination, 194(1), pp. 101-107.

Zhang, Z., Yu, H., Xu, M. & Cui, X. 2021. Preparation, characterization and application of geopolymer-based tubular inorganic membrane. Applied Clay Science, 203, p. 106001.

Zhao, X., Wang, T., Du, G., Zheng, M., Liu, S., Zhang, Z., . . . Gao, Z. 2019. Effective Removal of Humic Acid from Aqueous Solution in an Al-Based Metal–Organic Framework. Journal Of Chemical And Engineering Data, 64(8), pp. 3624-3631.

Zhou, J., Wandera, D. & Husson, S. M. 2015. Mechanisms and control of fouling during ultrafiltration of high strength wastewater without pretreatment. Journal Of Membrane Science, 488, pp. 103-110.

Zydney, A. L., 2016. Charged ultrafiltration membrane. In: Drioli, E. & Giorno, L. (eds.) Encyclopedia of Membranes. 1st ed. Heidelberg, Berlin: Springer. P. 372-373. ISBN 978-3-662-44325-5.